Perspective

# Towards the time-resolved spectroscopy of photoinduced electron dynamics in nuclear transitions

Marc Seitz [1] Francesca Calegari [1,2,3] Peter G. Thirolf [4] and Andrea Trabattoni [1,5,6]

[1] *Center for Free-Electron Laser Science CFEL, Deutsches Elektronen-Synchrotron DESY, Hamburg, Germany*

[2] *Department of Physics, Universität Hamburg, Hamburg, Germany*

[3] *The Hamburg Centre for Ultrafast Imaging, Universität Hamburg, Hamburg, Germany*

[4] *Ludwig-Maximilians-Universität München, Garching, Germany*

[5] *Leibniz University Hannover, Institute of Quantum Optics, Hannover, Germany*

[6] *Cluster of Excellence PhoenixD (Photonics, Optics, and Engineering-Innovation Across Disciplines), Hannover, Germany*

(Received 4 April 2025; published 8 October 2025)

The interaction between nuclear and electronic states plays a fundamental role in many nuclear processes. While such nucleus-electron couplings have been extensively studied using nuclear physics methodologies, recent advancements in light sources have introduced novel schemes for nuclear photoexcitation. This breakthrough enables a new class of experiments that could revolutionize our understanding and control of nuclear states. In this work, we review the research on electron processes associated with nuclear transitions, and the light sources that have been used for nuclear photoexcitation. Furthermore, we explore the potential for establishing time-resolved spectroscopy of electron-nucleus couplings, drawing connections to state-of-the-art light sources and time-resolved studies in atomic and molecular physics. By addressing both challenges and opportunities, we aim to provide a roadmap for future research in this interdisciplinary field. This emerging platform, linking nuclear science, atomic physics, and photonics, holds great promise for driving groundbreaking scientific and technological advancements.

DOI: 10.1103/31qf-pfvj

## I. INTRODUCTION

Electron dynamics play a fundamental role in the behavior of matter and underpin essential natural processes, such as electron transport chains in biochemistry [1,2] or charge transfer in energy-harvesting systems [3]. In atomic physics, electronic states and their mutual correlations are investigated, defining their general quantum mechanical properties. Electron processes are also pivotal to fundamental phenomena in nuclear physics. Nuclear states can exchange energy with surrounding electrons, and nucleus-electron couplings drive a large variety of nuclear decays that are of interest for scientific and technological applications. The electron-capture decay of $^{7}$Be, for example, serves as a promising observable for monitoring solar activity [4]. Similarly, electronic interactions influence the production and decay of medical isotopes such as $^{125}$I [5,6] and the relaxation of long-lived nuclear states relevant to high-precision metrology, as exemplified by $^{229}$Th [7–11].

The advent of advanced light sources has revolutionized our understanding of light-matter interaction, also enabling real-time observation of electron motion. Laser spectroscopy has provided unprecedented insight into fundamental processes such as photoionization, revealing, for example, the time required for electron ejection from an atom or the evolution of collective electron dynamics in plasmonic systems. Extending these methodologies to more complex systems has uncovered crucial aspects of molecular and material functionality, including photoprotection in biological molecules [12] and light-induced superconductivity [13]. These developments have also paved the way for novel control schemes at the quantum level, contributing to the emergence of fields such as quantum materials and metasurfaces [14,15]. Recent advances in large-scale and tabletop light sources have similarly transformed nuclear physics, enabling the external driving of nuclear transitions, an approach once considered conceptually unfeasible [16]. This breakthrough opens exciting possibilities for both fundamental science and technological applications [7–11].

We are now at a pivotal moment, with the unprecedented opportunity to harness modern light sources to advance our understanding of nuclear science. More importantly, it may soon be possible to establish time-resolved spectroscopy methods, already well established in other disciplines, to directly observe and manipulate the energy exchange between nuclear and electronic states. Figure 1 illustrates a prototypical experiment that may become feasible in the near future, employing the pump-probe concept [17]. A pump pulse resonantly excites a nuclear state, which subsequently releases energy into an atomic shell, triggering ionization. A probe pulse is then used to resonantly excite the same electronic state, perturbing the nucleus-electron interaction. By varying the delay between the pump and probe pulses, time-resolved snapshots of energy transfer between the nuclear and the

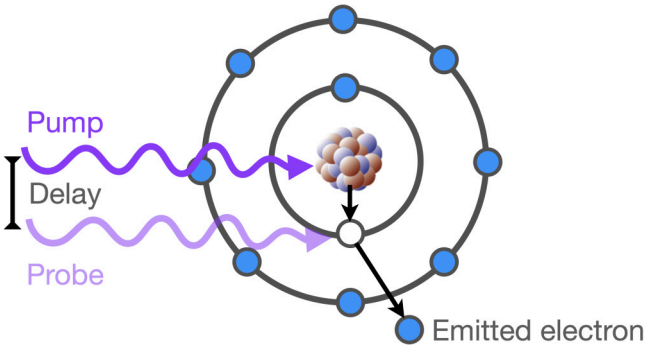


FIG. 1. A prototypical scheme of time-resolved pump-probe spectroscopy of photoinduced electron dynamics in nuclear transitions.

electronic state can be obtained. Beyond imaging and tracking nuclear dynamics in real time, a particularly promising application of this approach is the controlled excitation of nuclear states. By transiently altering electronic states through photoexcitation, it may be possible to precisely influence nuclear transitions and decay pathways.In this paper, we provide a comprehensive overview of the current state of research on electron processes associated with nuclear photoexcitation, drawing connections to the established time-resolved studies in atomic and molecular physics. As a key perspective, we examine the potential and limitations of adapting time-domain laser spectroscopy techniques, such as pump-probe schemes, to nuclear physics. We begin by reviewing recent technological advancements in novel light sources, both large scale and tabletop, that have been or could be utilized for nuclear state investigations. We then describe fundamental electron processes in nuclear physics, such as internal conversion, the electron bridge, and electron capture, emphasizing their roles in nuclear-electronic energy exchange. Next, we discuss the mechanisms governing electron dynamics in atomic and molecular physics, with a focus on time-resolved studies of electron correlations and nonadiabatic processes. Finally, we outline key milestones necessary to bridge electron dynamics studies in atomic and molecular physics with nuclear physics, laying the groundwork for time-resolved spectroscopy of nuclear transitions. By addressing these challenges and opportunities, this work aims to provide a roadmap for future research in this interdisciplinary field. The ability to study and control electron processes in nuclear transitions through light not only deepens our understanding of fundamental physics but may also offer innovative applications across various disciplines. As the field progresses, its integration with broader electron dynamics studies has the potential to create a new platform linking nuclear science, atomic physics, and photonics to drive groundbreaking scientific and technological advancements.

## II. LIGHT SOURCES FOR THE PHOTOEXCITATION OF NUCLEAR TRANSITIONS

This section reviews light sources that have been used, or have potential applications, for driving nuclear transitions. Historically, radioactive samples emitting gamma-ray radiation have been employed for the resonant excitation of nuclear states, for instance, within the framework of Mössbauer spectroscopy [18]. While this photointeraction scheme lies beyond the scope of our work, extensive reviews of resonant nuclear excitation via gamma-ray sources have been previously conducted [19–21]. With the significant advancements in large-scale facilities, such as synchrotrons and free-electron lasers (FELs), new pathways for photoexcitation of nuclear states have become accessible. These sources provide high-intensity x-ray pulses with multi-GW peak power, pulse energies reaching the millijoule range, and photon energies extending into the tens of keV [22]. This spectral region is well suited for triggering low-energy nuclear states in various isotopes, including iron-57 ($^{57}$Fe) at 14.4 keV and scandium-45 ($^{45}$Sc) at 12.4 keV. However, the narrow linewidths of these transitions, typically ranging from femtoelectronvolts (feV) to nanoelectronvolts (neV), do not align with the broader bandwidth of synchrotrons and FELs, which are on the order of hundreds of millielectronvolts (meV). Considerable research has focused on addressing these limitations, leading to significant progress over the last decade. Additionally, the excitation energy of these nuclear transitions is comparable to the resonant absorption of core atomic shells, often resulting in strong coupling between nuclear and electronic states. As a result, these photointeractions are relevant to this work and will be discussed in detail. A particularly notable example is the isomeric transition in thorium-229 ($^{229m}$Th), which stands out due to its exceptionally low excitation energy in the vacuum ultraviolet (VUV) spectral region (6.2–12.4 eV). The most recent measurements [23–25] place this transition at about 8.356 eV. With a radiative decay time on the order of $10^3$ s [26], this transition has attracted substantial interest over the past decades, particularly for its potential application in the development of a nuclear clock [10]. Considerable research has been devoted to triggering the direct photoexcitation of this transition using tabletop vacuum-ultraviolet coherent sources, with the ultimate goal of creating a high-precision metrology platform. Several laser technologies have reached maturity for this purpose, including cavity-enhanced high-harmonic-generation frequency combs and four-wave-mixing emission. These approaches will be reviewed in this work. Beyond these established methods, alternative schemes for the photoexcitation of nuclear states remain an area of interest for future exploration. Recent theoretical studies have proposed the use of strong-field lasers, twisted light, or continuous-wave radiation as potential mechanisms for nuclear excitation. These methods introduce additional degrees of control and could provide novel avenues for experimental investigation. Furthermore, the coherent control of long-lived electronic states has recently been extended from the optical to the extreme ultraviolet regime at FELs, suggesting a potential pathway for nuclear state population. The feasibility and implications of these approaches will be examined in the following sections.

### A. Bremsstrahlung and gamma-ray sources

Bremsstrahlung is produced when high-energy electrons are accelerated upon interaction with, for example, atomic nuclei or a magnetic field, resulting in a continuous spectrum

of photons extending up to the initial electron energy. This mechanism has been instrumental in nuclear resonance fluorescence (NRF) studies, where an excited nuclear state is resonantly populated through the absorption of electromagnetic radiation, followed by its decay via the emission of radiation. In photon-scattering experiments with bremsstrahlung, nuclear states across a broad energy range, extending up to the particle-separation energies, can be excited. Their subsequent deexcitation through electromagnetic transitions is analyzed using gamma-ray spectroscopy [27]. The key advantage of this technique is that both excitation and deexcitation occur through the well-understood electromagnetic interaction, making it a highly reliable method in physics [28].

A notable facility employing NRF is, for instance, the ELBE (Electron Linear Accelerator for beams with high Brilliance and low Emittance) at the Helmholtz-Zentrum Dresden-Rossendorf (HZDR) in Dresden-Rossendorf, Germany [29]. At the $\gamma$ELBE beam line, bremsstrahlung photons with energies up to 20 MeV at a repetition rate of up to 26 MHz are available and are mainly used in investigations on the electric or magnetic dipole strengths in nuclear transitions [30–34].

Advancements in photon sources have led to the development of Compton backscattering facilities, where optical photons are scattered off relativistic electron beams. This interaction results in a significant energy upshift, producing quasimonochromatic and highly collimated gamma-ray beams suitable for precise nuclear excitation studies. The High Intensity Gamma-ray Source (HI$\gamma$S) at Duke University, USA, exemplifies this approach [35]. By backscattering laser photons off electrons in a storage ring, HI$\gamma$S generates gamma rays with energies ranging from 1 to 100 MeV. This tunable source has been pivotal in various experiments on $\gamma$-ray spectroscopy, which has been used, for instance, for the investigation of nucleon structure and polarizability [35] or nuclear astrophysics [36].

In Europe, the Extreme Light Infrastructure-Nuclear Physics (ELI-NP) facility in Magurele, near Bucharest, Romania, is under development to provide advanced gamma-ray capabilities [37]. ELI-NP aims to produce gamma beams with energies up to 19.5 MeV and a subpercent bandwidth using laser Compton backscattering. This high-brilliance source is expected to enable a wide array of nuclear physics applications in industry [38], radioisotope production for medical applications [39], and precision spectroscopy [37].

Looking further ahead, the Gamma Factory initiative at CERN, proposed by Mieczyslaw Witold Krasny, Dmitry Budker, and collaborators, envisions utilizing the existing Large Hadron Collider (LHC) infrastructure to produce gamma rays through Compton backscattering off highly charged heavy ions circulating in the LHC ring [40]. This innovative approach could lead to ultra-high-intensity gamma sources, opening new avenues for research in atomic and nuclear physics [41] as well as fundamental particle physics for physics beyond the standard model [40].

While bremsstrahlung and gamma-ray sources provide valuable tools for NRF and nuclear excitation studies, their broad spectral width often limits energy resolution. To achieve higher precision in nuclear spectroscopy, x-ray synchrotrons offer a powerful alternative. By utilizing highly brilliant, and tunable x-ray beams, synchrotron facilities enable monochromatic excitation of nuclear transitions with superior spectral resolution. These properties and its applications will be presented in the following section.

### B. X-ray synchrotrons

Synchrotron radiation has revolutionized nuclear spectroscopy by providing highly brilliant, collimated, and monochromatic x-ray beams. Unlike conventional sources, synchrotrons generate radiation through high-speed electrons moving in circular accelerators, enabling precise studies of Mössbauer-active isotopes such as $^{57}$Fe. The Mössbauer effect is the recoilless nuclear resonance absorption and emission of gamma rays. A nucleus in an excited state emits a gamma quantum, which can be absorbed by another nucleus of the same kind, leading to resonance absorption and reemission (fluorescence) or conversion electron emission. In free atoms or molecules (gas, liquid), recoil from emission and absorption shifts the energy significantly, preventing resonance absorption. However, in solids, where atoms are bound in a lattice, recoil can be suppressed, allowing resonance absorption to occur. Rudolf Mössbauer experimentally confirmed this by cooling materials to low temperatures, where atoms remain largely stationary in the lattice, enabling recoilless emission and absorption [18]. Synchrotron-based Mössbauer techniques, implemented at facilities such as ESRF [42], SPRING-8 [43], and PETRA III [44], provide unprecedented insights into nuclear interactions and lattice dynamics, with applications in condensed matter physics, material science, and biophysics [45].

Two key Mössbauer techniques have been developed using synchrotron radiation, enabling advanced studies of nuclear and lattice dynamics. In nuclear resonant scattering (NRS), pulsed synchrotron radiation is used to excite nuclear states. The delayed reemission of radiation, detected via time-gated methods, reveals hyperfine interactions such as isomer shifts, electric field gradients, and magnetic fields [46]. Inelastic nuclear resonant scattering (INRS) extends Mössbauer spectroscopy to vibrational energy scales. By scanning the incident energy around the nuclear resonance, INRS selectively probes site-specific vibrational modes, providing direct insights into phonon dynamics [47].

One major breakthrough was the first observation of the phonon energy spectrum of polycrystalline $\alpha$-Fe, where nuclear resonant scattering was divided into elastic and inelastic events [48]. By tuning the energy of the incident synchrotron radiation, the phonon spectrum was directly measured, revealing shifts in nuclear energy levels due to phonon absorption and emission. The use of a pulsed synchrotron source allowed discrimination between nuclear resonant and nonresonant scattering, capitalizing on the long lifetime of the nuclear excited state in $^{57}$Fe [48,49]. These capabilities enable synchrotron-based Mössbauer spectroscopy to probe site-specific phonon dynamics with exceptional energy resolution.

Further advancements have demonstrated the potential of synchrotron radiation for studying conversion electron

emission following nuclear resonant excitation [46]. By monitoring delayed electron emission, researchers have been able to probe the phonon spectrum with depth resolution, as the small escape depth (approximately 200 nm) of low-energy electrons allows selective investigation of near-surface layers. Three primary processes contribute to the observed electron emission: the photoelectric effect, recoilless nuclear absorption followed by energy transfer to the electron shell, and inelastic absorption accompanied by phonon creation or annihilation [46]. A detailed review of [46] is reported in Sec. V.

Moreover, synchrotron radiation has enabled hyperfine structure analysis through quantum beats in the time spectrum of emitted gamma rays under coherent conditions [47]. Investigations of *K*-shell internal-conversion electron emission from $^{57}$Fe thin films deposited on Si(111) revealed modifications in the phonon density of states, with thinner films exhibiting softened phonon modes compared to bulk $\alpha$-Fe [47]. By employing high-resolution monochromators and time-resolved detection, these experiments distinguished delayed internal-conversion electrons from promptly emitted photoelectrons, further enhancing the ability to probe nuclear dynamics with unparalleled precision [47].

While synchrotron-based Mössbauer spectroscopy has been instrumental in studying hyperfine interactions and phonon dynamics, its capabilities extend beyond traditional Mössbauer-active isotopes, such as the isomeric nuclear transition in $^{229m}$Th. Given its potential for optical nuclear spectroscopy, synchrotron-based techniques offer a controlled approach to populating and probing its nuclear states with high precision. Masuda *et al.* [50] demonstrated the capability of synchrotron-based nuclear spectroscopy to precisely probe the low-energy nuclear transitions of $^{229}$Th. Using narrow-band 29-keV synchrotron radiation at SPring-8, they successfully excited $^{229}$Th to its second excited state. About 58% of the population in the second excited state subsequently decays in approximately 100 ps into the isomeric state. This marks the first instance of active optical pumping of $^{229m}$Th. The study established key nuclear parameters with unprecedented precision, determining the second excited state energy to be $29,189.93 \pm 0.07$ eV, measuring its half-life at $82.2 \pm 4.0$ ps, and extracting an excitation linewidth of $1.70 \pm 0.40$ neV. At the time of the publication, these results allowed for a refined estimation of the isomer's energy, confirming its location within a laser-accessible regime in the VUV region.

In summary, synchrotron-based Mössbauer spectroscopy has demonstrated remarkable capabilities in probing nuclear transitions, hyperfine interactions, and lattice dynamics with exceptional spatial, temporal, and energy resolution. By leveraging the tunability of synchrotron radiation, researchers have unlocked new insights into nuclear resonant scattering, phonon spectra, and photoexcitation of nuclear transitions. However, intrinsic characteristics such as the relatively long pulse durations and comparably low brightness impose limitations on peak intensities [51]. To address these challenges, free-electron lasers (FELs) have emerged as a groundbreaking alternative, providing ultrashort, coherent pulses with unprecedented peak brightness. The following section will explore the capabilities of FELs in greater detail.

### C. X-ray free-electron lasers

Apart from the particular case of the $^{229m}$Th isomeric transition, most other long-lived nuclear states that qualify as candidates for photoexcited nuclear spectroscopy have resonance energies on the level of tens of keV. These kinds of photon energies (0.01–10 nm, 100 eV-100 keV) are well within reach thanks to the advancements on x-ray free-electron laser (FEL) technology [22,51–56].

Free-electron lasers (FELs) combine particle accelerator and laser technologies to produce electromagnetic radiation with unparalleled brightness. They rely on relativistic electrons moving through a periodic magnetic field, generating undulator radiation [55]. Most FELs operate via self-amplified spontaneous emission (SASE), where small fluctuations in electron density grow as electrons interact with the emitted radiation, leading to the formation of microbunches spaced by the radiation wavelength [51]. When these electrons emit in phase, radiation intensity scales quadratically with the number of electrons, greatly enhancing output power [52,55]. In x-ray FELs, typical beam parameters (17.5 GeV electron energy, 5 kA peak current) enable peak radiation powers in the multi-GW range and pulse energies of a few millijoules, with a conversion efficiency of 0.1% [22].

The most recent breakthrough in nuclear transition spectroscopy has been achieved in an experimental beamtime conducted at the European x-ray FEL [22]. In this experiment, Shvyd'ko *et al.* [57] demonstrated the resonant excitation of the isomeric state in $^{45}$Sc by irradiation with x-ray photons. More than 30 years ago, the isomeric state of $^{45}$Sc was identified as one of the most promising nuclear targets for a nuclear clock due to its comparably low transition energy of 12.4 keV and long lifetime of 0.47 s. $^{45}$Sc predominantly decays via an internal conversion channel, resulting in the ejection of an electron from an inner shell. The successful excitation of the isomeric state can therefore be determined by detecting characteristic x-ray fluorescence at $K_\alpha = 4.09$ keV and $K_\beta = 4.46$ keV, which is emitted when the core hole from the internal conversion decay process is filled. By scanning the energy of the x-rays over a range of 100 eV around the nuclear resonance of 12.4 keV, it was possible to determine the transition energy of 12.38959 keV with an accuracy two orders of magnitude higher than previously measured values.

The potential realization of a $^{45}$Sc-based nuclear clock still requires major achievements, such as the development of a compact narrow-band x-ray frequency comb. However, the successful excitation of the $^{45}$Sc nuclear transition and the precise determination of its resonance energy underscore the potential of modern x-ray FELs in ultra-high-precision spectroscopy, nuclear clock technology, and metrology in the hard x-ray regime. With their high repetition rates and narrow bandwidths, state-of-the-art x-ray FELs provide a powerful platform for studying long-lived nuclear resonances.

While large-scale facilities such as synchrotrons and FELs provide the high-photon energies necessary for nuclear photoexcitation, their accessibility is limited due to beamtime constraints and operational costs. In contrast, table-top laser sources offer a promising alternative, enabling localized and

flexible experimental setups that are able to generate radiation in the vacuum and extreme ultraviolet, as well as the soft x-ray region through different nonlinear up-conversion processes. Especially table-top laser sources in the VUV have become particularly relevant in recent years, thanks to the new findings surrounding the low-energy nuclear transitions in $^{229}$Th. In the following, we discuss the potential of table-top VUV sources and their suitability for nuclear spectroscopy and photoinduced nuclear transitions.

### D. Table-top laser sources

The low-energy nuclear transition in the $^{229m}$Th isomer presents a promising avenue for advancing precision measurement technologies. Its unique properties, such as a low excitation energy and reduced sensitivity to external perturbations, make it an exceptional candidate for high-precision optical clocks and quantum sensing, with potential applications in ultra-accurate timekeeping and advanced metrology [9,58,59]. Realizing these applications, however, requires efficient and accessible laser sources in the VUV spectral region. This requirement has driven significant efforts toward the development of compact, table-top laser sources, which will be discussed in the following subsections.

*Up-conversion in nonlinear crystals.* To generate laser pulses with photon energies in the VUV spectral range, nonlinear optical interactions can be exploited to up-convert the lower frequencies of widely available laser sources, such as titanium:sapphire or ytterbium-based systems. One of the most common methods for frequency up-conversion of laser light involves the use of nonlinear crystals, which exploit second-order nonlinear effects such as second-harmonic generation (SHG) to achieve high-conversion efficiencies. In SHG, a monochromatic light wave with frequency $\omega$ propagates through a nonlinear medium, generating a new wave with twice the frequency $2\omega$. When the correct phase-matching conditions are chosen, the conversion efficiency between $\omega$ and $2\omega$ can be maximized [60,61].

Nonlinear crystals such as beta-barium borate (BBO) and lithium triborate (LBO) exploit this property and are widely used for SHG. These materials enable efficient frequency doubling of near-infrared or visible lasers, producing light in the visible (VIS, 400–750 nm, 1.65–3.1 eV) or ultraviolet (UV, 200–400 nm, 3.1–6.2 eV) spectral ranges with high (>50%) conversion efficiencies [61].

However, the applicability of nonlinear crystals for efficient frequency up-conversion is limited at higher-photon energies. As we move into the vacuum-ultraviolet (VUV) range, challenges arise due to intrinsic dispersion properties, material damage thresholds, and two-photon ionization limits. Additionally, the restricted transmittance of commonly used nonlinear crystals in the VUV region presents a significant obstacle [62].

To overcome these challenges, a novel technique was developed by Togashi *et al.* [63], utilizing prism-coupling of $KBe_2BO_3F_2$ (KBBF) crystals via optical contact, bypassing the need for index-matching fluids. While this crystal faces limitations, including low-conversion efficiency ($10^{-4}$) and material absorption that offers a theoretical cutoff wavelength of 147 nm [64], it enabled the generation of 163.3-nm pulses through sum-frequency mixing of a dual-frequency Ti:sapphire laser ($\omega_1 = 820$ nm producing 10-mJ, 50-fs pulses at a repetition rate of 10 Hz.

The material constraints make it clear that in the present time, nonlinear crystals are unable to provide a universal platform for table-top VUV generation, particularly in the context of photoexcitation of the $^{229}$Th nuclear transition. Aiming to resolve these issues, alternative approaches based on nonlinear wave mixing in gaseous media have gained significant attention. In particular, four-wave mixing (FWM) has emerged as a promising technique, offering high-conversion efficiencies, broader spectral coverage, and greater flexibility in wavelength tuning.

*Four-wave mixing.* Four-wave mixing (FWM) is a nonlinear optical process in which three interacting waves generate a fourth wave through a medium with a third-order nonlinear susceptibility ($\chi^{(3)}$) [60]. This process enables tunable frequency conversion making it a powerful tool for various applications, including VUV generation. A schematic representation of nondegenerate FWM is shown in Fig. 2(a).

As discussed in the previous chapter, the generation of VUV radiation using conventional nonlinear crystals is severely limited due to their intrinsic dispersion, low damage thresholds, susceptibility to two-photon ionization, and poor transmittance in the VUV spectral range. While high-harmonic generation (HHG) is widely used for shorter wavelengths (i.e., higher-photon energies), it suffers from low-conversion efficiencies in the relevant range. These limitations historically motivated the development of resonantly enhanced four-wave mixing as a preferred technique for generating tunable VUV light with comparatively high-conversion efficiencies on the order of 0.1%–0.2% [65–68]. This was made possible by the availability of rare gases such as xenon, which exhibit strong atomic resonances that can be exploited to boost the third-order nonlinear susceptibility. Early efforts on VUV light generation through resonance enhanced four-wave mixing FWM in xenon have established the basic feasibility of tunable coherent sources in the 120–220 nm range. For instance, the work by Hilbig and Wallenstein [65] achieved tunable VUV output between 155–220 nm with nanosecond dye lasers, but with conversion efficiencies typically below 0.2% and Ĩ kilowatt-level peak power. Later developments, such as for instance those by Tünnermann *et al.* [66] and Hanna *et al.* [67], improved the available VUV pulse energy and tunability, yet were either limited by achievable spectral linewidth on the THz level [66] or purposefully targeted at other applications such as aerosol spectrometry [67]. While it is true that FWM setups were optimized to achieve narrow linewidths on the order of 6-15 GHz [23,24,68], essential for addressing the ultranarrow thorium nuclear transition, the breakthroughs in photoexcitation of the isomeric transition of $^{229m}$Th by Elwell *et al.* and Tiedau *et al.* in 2024 are based on several key innovations that go beyond the development of resonance-enhanced FWM technology. For instance, the exact $^{229m}$Th transition energy, while continuously improving over time, remained uncertain within several eV until a more precise determination of the energy was provided only recently in different experiments. Seiferle *et al.* [69] conducted energy

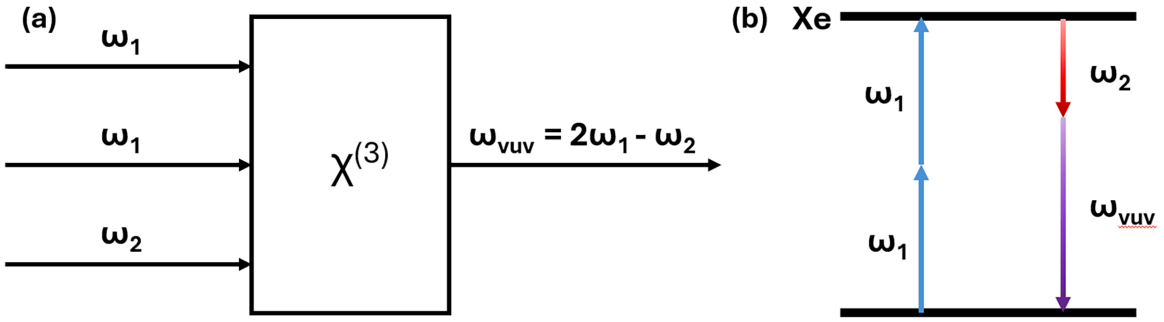


FIG. 2. Adapted from [60]. (a) Schematic of the third-order ($\chi^{(3)}$) nonlinear effect nondegenerate four-wave mixing. (b) Energy-level diagram for the nondegenerate four-wave mixing process in [68]. Two pump photons with frequency $\omega_1$ resonantly excite an atomic state in Xe. Frequency mixing with the second, tunable driving frequency $\omega_2$ results in frequency tunable VUV light ($\omega_{\mathrm{VUV}}$). The tunability is indicated with color gradients.

measurements of electrons emitted after internal conversion decay, Sikorsky *et al.* [70] presented $\gamma$-ray spectra produced in the $\alpha$-decay of $^{233}$U using a cryogenic microcalorimeter, and Kraemer *et al.* [26] performed vacuum-ultraviolet spectroscopy of $^{229m}$Th stemming from beta decay of $^{229}$Ac and embedded into $CaF_2$ and $MgF_2$ crystals. Especially the latter study was of strong relevance for the breakthroughs in nuclear spectroscopy of thorium because it achieved the first observation of the $^{229m}$Th radiative decay in large-band-gap crystals. The measured photon energy of 8.338 eV with an average statistical and systematic error of only 0.024 eV improved the uncertainty of the isomer's excitation energy by more than a factor of 7 compared to [69,70], drastically reducing the required scanning range for a VUV laser and therefore paving the way for the first successful observation of the radiative decay of the thorium isomer through photoexcitation with a FWM based VUV source one year later [23,24].

A comprehensive theoretical and experimental analysis of this third-order nonlinear process of FWM was presented by Bjorklund [71], providing valuable insight into the conditions required for efficient four-wave mixing. By examining different phase-matching configurations, specifically $\omega_1 + \omega_2 + \omega_3 = \omega_{\mathrm{VUV}}$, $\omega_1 + \omega_2 - \omega_3 = \omega_{\mathrm{VUV}}$, and $\omega_1 - \omega_2 - \omega_3 = \omega_{\mathrm{VUV}}$, Bjorklund demonstrated that while sum- and difference-frequency schemes (processes 1 and 3) require specific dispersion characteristics to achieve phase matching, the second process $\omega_1 + \omega_2 - \omega_3 = \omega_{\mathrm{VUV}}$ (used in most resonance-enhanced VUV generation schemes) can be phase matched in media with both normal and anomalous dispersion, thus also in presence of resonant absorption, making it broadly applicable and more easily optimized. Furthermore, the overall conversion efficiency of this FWM process can be significantly enhanced by tuning the pump wavelength to coincide with a two-photon resonance in the nonlinear medium. In the case of xenon gas, resonance at 249.6 nm greatly increases the third-order susceptibility $\chi^{(3)}$, thereby improving the conversion efficiency toward the VUV [72].

For instance, Tiedau *et al.* [23] used an experimental setup employing two Ti:sapphire continuous-wave (cw) lasers. The first emits light at 748 nm, which is frequency tripled through a cascaded process of second-harmonic generation (SHG) and sum-frequency generation (SFG) in two nonlinear crystals. The result is the pump wavelength of $\omega_1 = 249.6$ nm for resonant excitation of the two-photon transition $5p^6\ {}^1S_0 \rightarrow 5p^5(2P^{\circ}_{3/2})6p\ {}^2[1/2](J=0)$ in xenon. The energy-level diagram of this exemplary FWM process is depicted in Fig. 2(b). The second laser with frequency $\omega_2$ is wavelength tunable between 765 and 800 nm and is used to alter the difference frequency in the FWM process. This system generates up to 40 μJ of VUV pulse energy with a spectral linewidth of approximately 6 GHz in the range from 150 to 155 nm, maintaining a constant power level by selecting a suitable laser dye in their amplifier system. The VUV source operates at a repetition rate of 30 Hz, with a pulse duration of 10 ns and a mean pulse energy of approximately 15 μJ in the relevant wavelength range between 148.3 and 149.1 nm. A key element in the successful photoexcitation of the $^{229m}$Th isomer was the use of thorium-doped $CaF_2$ crystals, grown at TU Wien, featuring a $^{229}$Th concentration of up to $5 \times 10^{18}$ 1/cm$^3$. The groundbreaking results of this experiment include the first demonstration of photoexcitation of the $^{229}$Th nuclear transition, a reduction of the transition frequency by nearly three orders of magnitude [2020.409(7) THz, 148.3821(5) nm, 8.35574(3) eV], and a precise measurement of the isomer lifetime [1740(50) s] [23]. To clarify, this measured lifetime represents the expected vacuum value, inferred from measurements in a solid-state environment and scaled by $n^3$, assuming accurate knowledge of the refractive index at the relevant wavelength. While this assumption is likely reasonable, it does not constitute a direct measurement of the ionic lifetime in vacuum.

While noble-gas-based four-wave mixing has proven to be an effective method for generating coherent VUV radiation, its scalability and efficiency can be further enhanced by employing structured environments such as hollow capillary fibers. These waveguides provide higher interaction lengths, and increased confinement of the driving fields, leading to improved conversion efficiencies [62]. By leveraging the unique dispersion properties of hollow capillary fibers, four-wave mixing can be tailored to generate tunable VUV light, making it a promising platform for photoexcitation of nuclear transitions.

Building on these principles, Forbes *et al.* [73] presented their results on the generation of femtosecond VUV radiation via four-wave mixing in a noble-gas-filled HCF. This process involves two pump photons with frequency at 267 nm, one

seed photon with frequency at 800 nm, and the generated photon at the difference frequency $\omega_i = 2\omega_p - \omega_s$. The driving laser is a standard chirped pulse amplification Ti:sapphire laser with a pulse duration of 35 fs, a pulse energy of 2.7 mJ, and a repetition rate of 1 kHz. After splitting off one-third of the fundamental radiation to act as the seed for the FWM process later in the setup, the third harmonic of the laser is generated via a cascaded frequency up-conversion process in nonlinear crystals. The pump and seed pulses are then recombined and coupled into a 0.5-m-long helium-filled HCF with an inner diameter of 150 μm , where the FWM process is driven. The VUV pulses are characterized after the fiber, with a VUV photodiode enabling the measurement of pulse energy. For pump and seed powers up to 45 μJ , VUV pulse energies of approximately 4 μJ were obtained at the upper limit. This corresponds to a remarkably high conversion efficiency of around 10%, especially in comparison to other nonlinear processes. The temporal and spectral characterization of the VUV pulses was conducted through simultaneous yet separate measurements, revealing a VUV spectrum with a full width at half-maximum (FWHM) of approximately 1.1 nm, corresponding to a transform-limited pulse duration of 35 fs.

*Cavity-enhanced HHG and frequency combs.* High-harmonic generation (HHG) is a highly nonlinear optical process that enables the generation of coherent light at extreme ultraviolet (XUV, 10–124 nm, ; 10–124 eV) or even soft x-ray wavelengths (0.1–10 nm, 124 eV–10 keV). This process typically occurs when an intense laser field interacts with atoms or molecules in a gaseous medium. The microscopic dynamics underlying HHG can be explained by the three-step model [74,75]. HHG occurs when an intense laser pulse (with peak intensities of around $10^{14}$ W/cm$^2$) [60] interacts with a medium. In the framework of a single-atom picture, the laser's electric field distorts the Coulomb potential of the atom, enabling tunnel ionization for outer electrons. The ionization probability is highly time localized, occurring near the laser field peaks. After ionization, the electron is accelerated by the laser field, eventually recombining with the ion and emitting high-energy photons. The emission is linked to the electron's instantaneous acceleration due to the Coulomb potential. In a collection of atoms, the emitted radiation forms a coherent pulse train, spaced by half the optical period of the driving field. Fourier transforming this pulse train generates a harmonic spectrum with components spaced by twice the laser frequency, leading to odd-order harmonics. The spectrum can extend into the XUV and soft x-ray regions depending on the laser intensity and wavelength [60,76].

While traditional HHG has proven to be a powerful tool for generating ultrashort, XUV laser light, it also presents challenges in terms of maximum achievable power and tunability. To address these limitations, novel approaches have been developed, one of which involves the use of frequency combs. One such innovation is intracavity HHG [77,78], where a high-average-power infrared frequency comb, delivering femtosecond pulses at MHz repetition rates, is coupled to a dispersion-controlled optical cavity.

A frequency comb is a laser technology that generates a spectrum with evenly spaced frequency lines, created by a mode-locked laser emitting ultrashort pulses at a fixed repetition rate. The comb frequencies are described by $f_n = nf_{\text{rep}} + f_0$, where $f_{\text{rep}}$ is the pulse repetition rate and $f_0$ is the carrier-envelope offset frequency. The mode-locking process synchronizes the laser's longitudinal modes, producing a regular pulse train and a discrete frequency spectrum. Stable frequency combs can be linked to an external reference, such as an atomic clock, by stabilizing both the repetition rate and $f_0$ [79]. The carrier-envelope offset arises due to dispersion in the laser cavity, leading to a phase shift between the carrier wave and pulse envelope. This shift is quantified by the carrier-envelope phase slip $\Delta\phi_{ce}$, and results in a frequency offset $f_0 = f_r\Delta\phi_{ce}/2\pi$. Stabilizing $f_0$ is critical for accurate comb generation. While this led to the development of various techniques over the years [80–82], most commonly the "f-2f" interferometer is used, which combines supercontinuum generation, frequency doubling, and interferometry for feedback control [79,83].

Building on the success in precision spectroscopy and metrology, frequency comb technology has been extended into high-energy photon generation. By combining the precision and coherence of frequency combs with nonlinear optical processes, researchers have pushed their applicability into the extreme ultraviolet (XUV) and soft x-ray regions, bringing us back to intracavity HHG [77,78]. Coupling a frequency comb into a dispersion-controlled optical cavity enables phase matching for high-harmonic generation, leading to the formation of a unique comb structure within each harmonic, preserving the repetition frequency of the driving pulse train. This approach allows the generation of coherent light with photon energies ranging from 8 to 30 eV [77].

The demand for coherent, narrow-band light in the vacuum ultraviolet (VUV) spectral region, combined with the need for precise frequency control, makes frequency combs a promising tool for addressing the challenges in investigating the photoinduced nuclear transition in $^{229}$Th. Zhang *et al.* [78] demonstrated a tunable VUV frequency comb by coupling a high-repetition-rate femtosecond frequency comb (central wavelength ∼1040 nm) into a femtosecond enhancement cavity. This setup generated VUV light via intracavity HHG, producing coherent harmonics spanning photon energies from 7.4 to 9.8 eV. The system achieved linewidths on the kHz level, making it suitable for high-resolution spectroscopy of the nuclear transition. In a subsequent study, Zhang *et al.* [25] used this VUV frequency comb to precisely measure the energy of the $^{229m}$Th nuclear isomeric transition by referencing it to a stabilized optical clock in $^{87}$Sr. The direct excitation of $^{229\text{m}}$Th nuclei and the observation of generated fluorescence of ∼8.4 eV (∼148 nm) enabled the measurement of the isomeric transition energy with unprecedented precision.

Furthermore, a high-power VUV frequency comb laser system is currently under development at the Fraunhofer ILT in Aachen as part of the ThoriumNuclearClock ERC Synergy project [84]. This system is designed to generate VUV radiation at 148 nm with a bandwidth of approximately 2 nm. The output parameters of an infrared frequency comb at 1050 nm, with a 40-MHz repetition rate, will be enhanced with a combination of amplification and postpulse compression in order to generate high harmonics efficiently in a xenon gas jet, while preserving the laser's narrow linewidth. The system is expected to provide an average VUV comb power of $\geqslant 0.35$ mW, sufficient to excite the nuclear transition when tightly

focused onto thorium ions confined in a linear Paul trap. This laser system is anticipated to be a key component of the first prototype of a nuclear clock based on the $^{229m}$Th isomer [85].

In summary, the precision and coherence of frequency combs, particularly when combined with intracavity high-harmonic generation, have proven to be and will continue to be instrumental in advancing nuclear spectroscopy of $^{229}$Th.

*Resonant dispersive wave emission.* In the context of successful nuclear photoexcitation of $^{229m}$Th with table-top lasers, the reported laser intensities and measured lifetimes from Refs. [24,25] correspond to a relatively low Rabi frequency. Coherent control of the nuclear state would require a much higher power in the VUV range [25]. Apart from fiber-based four-wave-mixing approaches that were already presented, another promising avenue for addressing this challenge lies in the use of resonant dispersive wave emission within hollow-core fibers.

When highly intense optical pulses propagate in a nonlinear, dispersive medium, they undergo modifications due to self-phase modulation (SPM). This process induces variations in the instantaneous frequency of the pulse, resulting in a spectral broadening due to intensity-dependent changes in the refractive index. Group-velocity dispersion (GVD) further affects pulse shape by causing different frequency components to propagate at different speeds, depending on the sign of the GVD parameter $\beta_2$. To quantify the effects of SPM and GVD and mathematically describe the propagation of light pulses through nonlinear, dispersive media, one can employ the nonlinear Schrödinger equation, where temporal pulse broadening due to GVD competes with spectral pulse broadening due to SPM. Under specific conditions, it is possible to achieve complete compensation of both effects, leading to the formation of optical pulses that remain invariant to SPM- and GVD-induced changes, known as temporal optical solitons [60].

Optical soliton dynamics play a crucial role in a variety of nonlinear optical phenomena, particularly in fiber optics. Common applications include pulse compression [86], supercontinuum generation [87], and resonant dispersive wave (RDW) emission [88,89] in gas-filled hollow-core fibers (HCF). Among these, RDW emission is particularly noteworthy, as it enables the generation of few-femtosecond laser pulses that are tunable from the vacuum ultraviolet (VUV) to the near infrared [90]. The dispersion properties of a hollow capillary fiber can be tailored by adjusting the GVD parameter $\beta_2$, which depends on the wavelength $\lambda$ and gas pressure $p$ in the waveguide. In HCFs, the total GVD profile results from both waveguide dispersion and gas dispersion. The waveguide dispersion of an evacuated capillary is always anomalous ($\beta_2 < 0$) across all wavelengths, whereas the gas dispersion is normal ($\beta_2 > 0$) from the ultraviolet to the near infrared. By adjusting the gas pressure, one can control the total dispersion profile [91]. The wavelength of the RDW depends on the pump wavelength relative to the zero-dispersion wavelength of the waveguide, which is influenced by the gas type, pressure, and fiber core diameter. By tuning these parameters, phase matching of RDW emission can be achieved over a broad spectral range (110–350 nm), generating pulse energies at tens of microjoules in the VUV range between 107–180 nm [89]. Numerical simulations suggest that this process can be scaled by at least one order of magnitude, potentially generating up to 300 μJ of VUV pulse energy with peak powers exceeding 80 GW. If realized experimentally, a table-top laser source based on RDW emission could surpass free-electron lasers (FELs) in peak brightness within the VUV spectral region [89].

Given the increasing advancements in fiber laser systems and their ability to efficiently generate VUV light, resonant dispersive wave emission could play a key role in scaling up the power of VUV lasers for precise nuclear excitation. This would provide a new approach for achieving the necessary high-intensity fields to probe and manipulate nuclear states with unprecedented control.

To provide a structured comparison of the various approaches for vacuum ultraviolet (VUV) generation, the following table in Fig. 3 summarizes the typical parameter ranges achieved across the main schemes discussed: nonlinear crystal-based generation, resonance-enhanced four-wave mixing (FWM), cavity-enhanced high-harmonic generation (HHG), and VUV frequency combs, as well as resonant dispersive-wave (RDW) emission. The comparison includes key laser characteristics relevant for VUV-driven experiments, namely, spectral bandwidth, pulse energy, repetition rate, and conversion efficiency from the laser driver.

### E. Novel routes for the photoexcitation of nuclear states

The above-mentioned approaches of nuclear photoexcitation have relied on comparably broadband VUV sources, FELs, or synchrotron radiation, but these methods often suffer from low efficiency, limited spectral resolution, or impractical experimental constraints. To overcome these challenges, novel excitation schemes are being proposed that leverage advances in laser physics, structured light fields, and quantum control techniques.

In this section, we present three promising approaches: photoexcitation with twisted light, which exploits the unique properties of orbital angular momentum to enhance nuclear coupling; continuous-wave VUV lasers, which offer the spectral precision and stability necessary for resonant nuclear excitation; and rapid adiabatic passage, a robust quantum control method that enables efficient population transfer even in the presence of spectral uncertainties. In the near future, these techniques could represent significant steps toward photoexcitation of nuclear transitions.

*Photoexcitation with twisted light.* Twisted light, also known as optical vortex beams, is a special type of structured light that carries orbital angular momentum (OAM). Unlike conventional plane waves, which have a uniform phase front and carry only spin angular momentum (SAM) determined by their polarization helicity (e.g., circular polarization), twisted light features a helical wavefront (vortex beams), that gives rise to a spatially varying intensity and momentum distribution [92–94]. While SAM is an intrinsic angular momentum associated with polarization of plane wavefronts, OAM is a spatial degree of freedom, arising from the beam's transverse phase structure, allowing twisted light to interact with matter in fundamentally different ways than plane waves. While extensively studied in atomic physics [95–97], its application in nuclear physics remains largely unexplored, particularly in the context of nuclear clock transitions.

| VUV output parameter | Spectral bandwidth | Pulse energy | Repetition rate | Conversion efficiency |
|---|---|---|---|---|
| Nonlinear crystals | ~ 100s of GHz – few THz | ~ pJ – nJ | ≤ kHz | $\leq 10^{-4}$ |
| Resonance enhanced FWM | ~ 10s of MHz – few THz | ~ 10s of μJ | ~ 10s of Hz – kHz | $\leq 10^{-2}$ |
| Cavity enhanced HHG, VUV combs | ~ 300 kHz – 10s of THz | ~ pJ – nJ | ~ 10s – 100s of MHz | $\leq 10^{-5}$ |
| RDW | ~ 10s – 100s of THz | ~ 10s of μJ | ≤ 10s of kHz | $\leq 10^{-1}$ |

FIG. 3. Comparison of the VUV generation schemes that were described in previous subsections and their typical output parameters.

In a recent work, Kirschbaum, Schumm, and Pálffy [98] investigated the feasibility of using twisted light to drive the 8-eV nuclear clock transition in $^{229}$Th. Their study considered two experimental scenarios: excitation of a single trapped $^{229}$Th ion and excitation of an ensemble of $^{229}$Th nuclei embedded in a $CaF_2$ crystal. Using a density matrix formalism, they calculated nuclear excitation probabilities and analyzed the effects of twisted light on the transition selection rules.

In the case of a single ion, they show that the excitation probability depends on the impact parameter, i.e., the relative position of the nucleus with respect to the phase singularity of the twisted light beam. A particularly striking result is that, on axis (zero impact parameter), twisted light can suppress the magnetic dipole (M1) transition and selectively excite the electric quadrupole (E2) transition, a feature that cannot be achieved using plane waves. When the ion is placed off axis, a mixture of M1 and E2 transitions occurs, but with altered relative strengths compared to conventional excitation schemes. Similar experimental findings, supported by a complete theoretical framework, were presented by Solyanik-Gorgone *et al.* [99], where single $^{40}Ca^{+}$ ions interacted with tailored, twisted electromagnetic fields.

For the case of ensemble excitation in a $CaF_2$ crystal, the study takes into account the effects of quadrupole splitting induced by the crystal lattice, which affects the orientation of the nuclear quantization axes. The results suggest that while twisted light interacts differently with nuclei aligned along different crystallographic directions, the overall excitation probability remains comparable to that of a plane wave in many configurations. Nonetheless, the findings indicate that structured light beams could provide additional degrees of freedom for nuclear excitation control in solid-state nuclear clocks.

The uniqueness of this work lies in the demonstration that twisted light can alter the selection rules governing nuclear transitions, enabling a level of control that was previously unattainable. By leveraging the structured phase properties of twisted light, the study proposes a method to suppress or enhance specific nuclear transition pathways, which could be advantageous for future precision spectroscopy experiments on $^{229}$Th. These results provide a theoretical foundation for future experimental efforts and suggest that structured light beams could be used to optimize nuclear excitation schemes, particularly in the context of developing a nuclear clock. To implement these findings in an experimental setting, the first challenge would be the development of coherent, tunable twisted light sources in the VUV regime. For trapped ion experiments, precise control over the impact parameter between the ion and the twisted beam's phase singularity would be necessary to exploit the unique selection rules predicted in the study. In the crystal-based approach, careful control over doping processes and crystallographic orientation could help tailor the nuclear excitation process to take full advantage of twisted light properties.

*Continuous-wave VUV lasers.* In the subsection on frequency up-conversion in nonlinear crystals, solid-state VUV lasers were introduced as one of the possible drivers for the nuclear transition in $^{229}$Th. While the generation of pulsed-VUV laser light has been achieved, an ideal laser for this application would be stable, narrow-band (mHz bandwidth), and continuous wave (cw) [100]. At the same time, the intrinsic limitations of currently used nonlinear crystal materials have been presented. Apart from that, the generation of cw-VUV radiation in a similar scheme as in the already presented Ref. [63] via SFG would require highly intense cw-laser drivers below 190 nm, which currently do not exist [100].

In an effort to find the key to solid-state VUV generation, different materials that display nonlinear optical behavior have been investigated. In their research paper, Herr *et al.* [101] have presented one promising candidate, which is $BaMgF_4$ (BMF). BMF is a ferroelectric, nonlinear material with a transparency range between approximately 130 nm to 13 μm [101]. Because BMF is a ferroelectric crystal, one can access the full transparency range for frequency conversion processes by exploiting quasiphase matching (QPM) through electric-field poling. By moving a metal tip over the crystal while applying a high voltage, they achieved domain inversion and identified an angular bandwidth for which high-quality poling occurs without degradation. This marks the first successful demonstration of nonparallel domain poling in BMF, crucial for tunable all-solid-state VUV sources [101].

These findings have major implications for cw-VUV lasers. BMF's broad transparency range, resistance to photodarkening, and nontoxic nature make it a strong alternative to

KBBF, which requires prism coupling [63]. Future research should focus on miniaturizing QPM periods and optimizing poling techniques to unlock BMF's full potential for compact, tunable VUV laser sources, with applications in precision spectroscopy and photoexcitation of nuclear transitions.

*Coherent control schemes.* Rapid adiabatic passage (RAP) is a well-established quantum control technique that enables highly efficient and selective population transfer between two quantum states [102]. In essence, RAP relies on sweeping the frequency of a driving field in a controlled manner, for example, by introducing a linear chirp to the driving laser field, ensuring that the system follows its instantaneous eigenstate without undergoing nonadiabatic transitions. For the efficient excitation of a nuclear excited state, RAP presents a promising alternative to direct resonant excitation, as it would circumvent the need for a narrow-band laser source while still achieving a very high population efficiency. Similar coherent control schemes for nuclear state population transfer, including the use of partially overlapping x-ray pulses, have been investigated theoretically in the context of the $^{229}$Th isomer [103].

In a RAP scheme, a driving laser field that could be considered broadband with respect to the linewidth of the nuclear excited state would be applied to adiabatically sweep through the resonance of the nuclear transition. The key requirement is that the interaction remains within the adiabatic regime. This means that the modulation in laser frequency has to be much slower than the period of the Rabi frequency of the transition, but at the same time shorter than the lifetime of the excited state to avoid unwanted decoherence or relaxation processes [102]. Quantitatively, this condition is typically expressed as $\Omega\tau \gg 1$, where $\Omega$ is the peak Rabi frequency and $\tau$ the pulse duration. A concrete example is provided by Kuznetsova *et al.* [104], who demonstrated efficient two-photon population transfer to a Rydberg state using chirped pulses of $\tau \sim 0.4\,\mu$s duration and Rabi frequencies on the order of $\Omega = 2\pi \times 30$ MHz. This yields $\Omega\tau \sim 100$, satisfying the adiabaticity condition. Moreover, the pulse duration remained well below the radiative lifetime of the excited Rydberg state (tens to hundreds of microseconds), allowing high-fidelity population transfer without significant spontaneous decay.

It is true that aspects, such as the chirp rate and adiabaticity, noise on either the energy states or the frequency of the driving laser [105], as well as dissipation effects [106] are remaining challenges to achieve RAP for nuclear transitions. At the same time, solutions to circumvent these issues are investigated and modeled, while earlier theoretical works such as Bürvenich *et al.* [107,108] or Liao *et al.* [109] further support the idea that indeed, femtosecond to attosecond x-ray lasers, particularly seeded FELs or XFELs, may in future be used to coherently control nuclear transitions.

Implementing RAP in a real experimental setup for nuclear excitation of $^{229}$Th could follow a two-step approach. First, $^{229}$Th atoms or ions need to be provided in a well-defined environment, for example, in a solid-state, high-band-gap host such as $CaF_2$ crystals [110]. Second, the laser pulses of a VUV laser system, based on one of the many proposed technologies in this chapter, would be modulated to sweep across the nuclear resonance frequency. The presence of RAP-induced coherent excitation could be verified by monitoring, for instance, fluorescence photons or internal conversion electrons with characteristic energies.

## III. ELECTRON PROCESSES IN NUCLEAR PHYSICS

This section reviews electronic processes in nuclear transitions, providing an overview of current knowledge and past and ongoing research. Specific examples where electron processes are essential to high-interest nuclear transitions, such as internal conversion in the decay of the isomeric state of $^{229}$Th [25,58] or in Mössbauer isotopes like $^{57}$Fe [111] or $^{45}$Sc [57], are discussed. Other electronic processes relevant for nuclear transitions are also presented, i.e., nuclear excitation by electron capture (NEEC), nuclear excitation by electronic transition (NEET), and electronic bridge (EB).

### A. Internal conversion

Driving nuclear transitions via coupling to the atomic shell is one of the most intriguing ways for the manipulation of nuclear states. Of particular interest is the internal conversion (IC) process, a nuclear deexcitation mode which competes with gamma emission. In the process of IC, nuclear excitation energy is transferred to a bound electron in the atom, which is then ionized, emitting so-called conversion electrons [112]. Internal conversion is favored whenever the energy available for a gamma transition is small, and it is also the primary mode of deexcitation for $0^+ \rightarrow 0^+$ (i.e., E0, electric monopole) transitions, where $\gamma$ decay is forbidden in all orders of the multipole expansion due to angular momentum and parity conservation [113]. It is of particular importance in heavy nuclei, as the IC decay rate scales with $Z^3$. The competition between IC and gamma decay is quantified in the form of the internal conversion coefficient $\alpha$ which is defined as $\alpha = \Gamma_e/\Gamma_\gamma$, where $\Gamma_e$ is the rate of decays via the emission of conversion electrons and $\Gamma_\gamma$ is the rate of gamma-ray emission observed from a decaying nucleus [113]. A prominent example is the isomeric first excited state of $^{229}$Th, with a uniquely low-excitation energy of about 8.356 eV, representing the lowest nuclear excitation presently known. Therefore, radiative decay is strongly suppressed, resulting in a rather long lifetime of the 'thorium isomer $^{229m}$Th of about 2000 s [23]. The ratio of the radiative decay width to the ground-state transition energy is presently estimated at $\Gamma_\gamma/E_{\rm iso} \approx 10^{-19}$. Given this very narrow width and the high resilience of nuclei to external perturbations (due to the small nuclear moments compared to the about $10^5$ larger atoms) [114], the isomeric state has been proposed for applications such as a nuclear frequency standard (nuclear clock) with unprecedented accuracy [8,114,115], a nuclear laser [116], or coherent control of the nuclear excitation via the electronic shell [117]. As a result of the low-excitation energy, the thorium isomer can decay via three decay channels to its ground state, whose occurrence depends on the electronic environment of the nucleus [118–121]: when the binding energy of an electron $E_B$ in the atomic shell of the nucleus is lower than the excitation energy of the isomer $E_{\rm iso}$, the isomer decays preferably via internal conversion (IC) [122] by emitting a conversion electron with an energy $E_e = E_{\rm iso} - E_B$. Alternatively, the deexcitation could proceed via $\gamma$ decay (emission of a VUV photon). Another

possible decay channel is bound internal conversion (BIC), where the nuclear decay energy is also transferred to the electronic shell. Instead of an electron being emitted, as in the internal conversion decay, an electronic state is excited [123]. Since the nuclear excitation energy of the thorium isomer $^{229m}$Th (8.356 eV) lies above the first ionization threshold of Th (6.30670 eV [124–126]), the ground-state decay of the nuclear excited state from a neutral atom can occur not only radiatively but also via internal conversion (IC), while this decay branch is energetically suppressed in ionic charge states of $^{229m}$Th (second ionization potential in Th: 12.1 eV [125,126]). Due to the large internal conversion coefficient of $\alpha \approx 10^9$ the partial IC lifetime is accordingly reduced to 7(1) µs [127,128]. In these experiments, where initially charged $^{229m}$Th$^{q+}$ ions were neutralized on metallic surfaces to trigger the IC decay, indications of a dependence of the IC decay lifetime on the electronic environment were seen, motivating still ongoing studies of the lifetime of $^{229m}$Th when being neutralized on metallic surfaces with different work functions. The radiative decay of $^{229m}$Th escaped experimental observation for decades and hence the first direct observation of the $^{229m}$Th ground-state decay was realized via IC electron detection following the $^{233}$U $\alpha$ decay, feeding with a 2% decay branch into the thorium isomer [58]. Also, the first precise direct determination of the $^{229m}$Th excitation energy was achieved by conversion electron spectroscopy [127]. Only recently the VUV fluorescence decay of $^{229m}$Th could be identified first from implanted $^{229}$Ac nuclei (which $\beta$ decay into $^{229(m)}$Th) in different large-band-gap crystals ($CaF_2$, $MgF_2$) [26] and subsequently also directly via resonantly irradiating highly $^{229}$Th-doped VUV transparent, large-band-gap crystals with a broadband laser [23,24] and a narrow-band VUV frequency comb [25], respectively. However, as these isomer excitation schemes require highly sophisticated laser systems that operate in the experimentally unfavorable VUV wavelength regime, alternative scenarios involving electrons in the atomic shell could relax the experimental challenges considerably. Consequently, excitation processes of the thorium isomer $^{229m}$Th via coupling to electrons have also been extensively studied [129], for example, via electronic bridge (EB) processes [130–136], inelastic scattering of electrons [137,138] or muons [139], and laser-driven electron recollision [140–142].

### B. Nuclear excitations by electron processes in Mössbauer isotopes

It is a long-standing challenge: Is it possible to fully excite an ensemble of atomic nuclei using externally applied electromagnetic fields [143]? This question relates to the goal of building a $\gamma$-ray laser ("graser"), with inverted nuclei as a gain medium, which was proposed long ago after the laser-maser principle [144]. The discovery of the Mössbauer effect, allowing for the recoil-less absorption and emission of $\gamma$-ray photons from certain nuclei [145], further stimulated this research field. While in the early 1990s efforts were directed towards developing lasing without inversion [146], by the end of the decade most approaches towards realizing a $\gamma$-ray laser were deemed unfeasible [147]. However, revisiting the initial goal of the graser appears appropriate due to (i) recent x-ray source advances (like the XFEL technology) and (ii) advances in using Mössbauer isotopes for demonstrating quantum optical concepts in the regime of hard x-rays, like superradiance [148], electromagnetically induced transparency in a cavity [111], vacuum-assisted generation and control of atomic coherences [149], interferometric phase detection [150], tunable subluminal propagation of narrow-band x-ray pulses [151], collective coupling of x-rays and nuclei in a nuclear optical lattice [152], Rabi oscillations of x-ray radiation between two nuclear ensembles [153], or coherent control of the waveforms of recoilless $\gamma$-ray photons [154].

Advances in x-ray source technology such as x-ray free-electron lasers (XFEL) [55,155] have stimulated the study of high-energy nonlinear effects in atoms, analogous to the groundbreaking development at lower photon energies following the invention of conventional laser sources. Various nonlinear x-ray processes have already been observed involving electronic transitions [156–160]. Also lasing on an inner-shell electronic transition based on XFEL-generated inversion has been demonstrated [161]. This raises the question if the source advances provide new approaches for the excitation of nuclei. Moreover, Mössbauer nuclei have evolved into a promising platform for quantum optics at energies of hard x-rays. The extremely narrow linewidth of Mössbauer transitions renders them ideal candidates for applications in precision spectroscopy and quantum optics, as detailed in the overview and reviewing publications [162–164]. Most commonly associated with the study of hyperfine interactions in solid-state targets, recent years have witnessed a rising interest in Mössbauer nuclei as an experimental platform for studying and controlling quantum dynamics and quantum optical effects [165]. The manipulation of light-matter interactions by controlling atomic levels enables many applications in optical sciences (see [111] and references therein). The key underlying technique is electromagnetically induced transparency (EIT), where quantum interference between electronic transitions turns an opaque medium transparent near an atomic resonance [166]. With the advent of high-brilliance, accelerator-driven light sources such as storage rings or (FEL-based) x-ray lasers, it has become attractive to extend the techniques of optical quantum control to the x-ray regime [167,168]. As a prototypical example, in [111] nuclear electromagnetically induced transparency in the regime of hard x-rays was demonstrated, using the two-level system of the 14.4-keV nuclear resonance of the Mössbauer isotope $^{57}$Fe (neglecting the nuclear hyperfine interaction). The key to the realization of nuclear EIT demonstrated in [111] was cooperative emission from ensembles of Mössbauer nuclei that were properly placed in a planar cavity for hard x-rays provided by synchrotron radiation from the PETRA III synchrotron radiation source of DESY (Hamburg). The radiative coupling of the nuclear ensembles by the cavity field establishes the atomic coherence necessary for the cancellation of resonant absorption. Because this technique does not require atomic systems with a metastable level, electromagnetically induced transparency and its applications can be transferred to the regime of nuclear resonances, establishing the new field of nuclear quantum optics [111]. The nuclear resonances of Mössbauer isotopes exhibit extremely narrow energy references for high-resolution spectroscopy, especially in the field

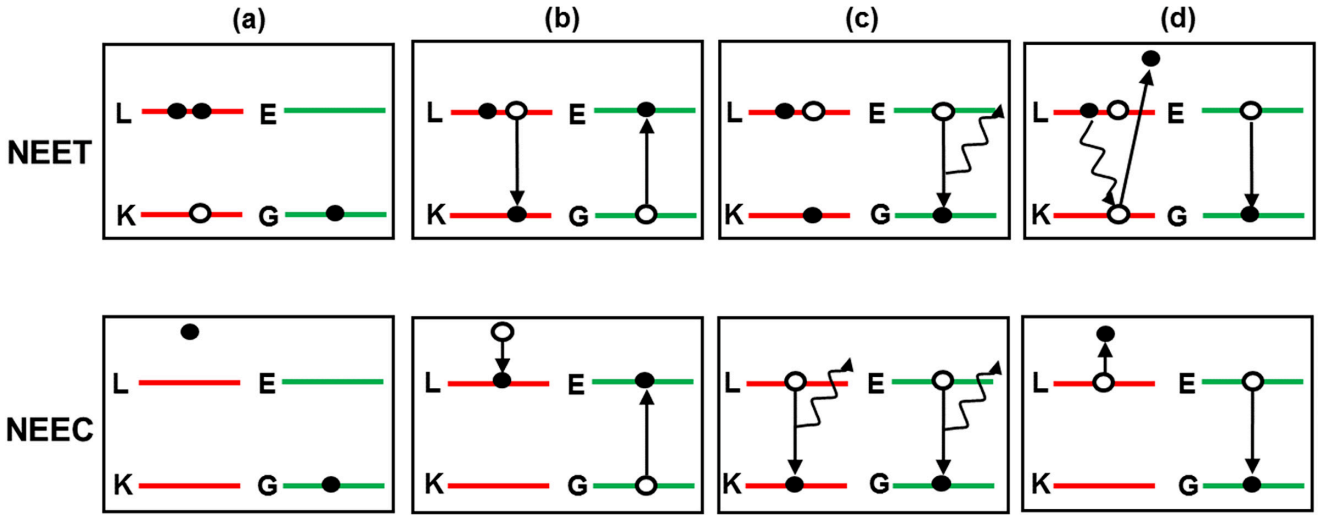


FIG. 4. Illustration of the nuclear excitation by electron transition (NEET) and nuclear excitation by electron capture (NEEC) processes. (a) The nucleus is in the ground state (G), the atomic shell has vacancies. (b) Electrons are captured and transition into atomic states and the nucleus is excited. (c) The nuclear excited state decays via $\gamma$-ray emission (the $K$ vacancy is filled from the $L$ shell with x-ray emission). (d) The nuclear state decays via internal conversion and electron emission.

of extreme metrology with applications to probe fundamental physics. Ultranarrow nuclear transitions are particularly suited for such applications due to their inherent insensitivity to external perturbations as compared to electronic levels. Hence, another candidate for a nuclear clock isomer is the ultranarrow nuclear resonance transition in $^{45}$Sc between the ground state and the 12.4-keV isomeric state with a lifetime of 0.47 s [169]. The scientific potential of $^{45}$Sc was realized long ago, but applications require $^{45}$Sc to be resonantly excited. This necessitates, in turn, accelerator-driven, high-brightness x-ray sources that have become available only recently, e.g., with the European XFEL at DESY in Hamburg [22,170]. Recently, resonant x-ray excitation of the $^{45}$Sc isomeric state could be demonstrated by irradiation of a Sc-metal foil with 12.4-keV photon pulses from a state-of-the-art x-ray free-electron laser and subsequent detection of nuclear decay products [57]. X-ray free-electron lasers promise a substantial enhancement of the number of nuclear-resonant photons per pulse, such that excitations beyond the low-excitation energy regime come within reach. Closest to internal conversion discussed before, its inverse process nuclear excitation by electron capture (NEEC) will be introduced next, followed by nuclear excitation by electron transition (NEET). These processes can provide very efficient nuclear excitation mechanisms for small transition energies and are expected to play an important role in dense stellar (as well as high-power laser-induced) plasmas. These processes are schematically illustrated in Fig. 4. Couplings between atomic and nuclear degrees of freedom are also expected to play an important role in the context of nuclear isomers, i.e., long-lived excited nuclear states like the previously discussed $^{229m}$Th.

### C. Nuclear excitation by electron capture (NEEC)

In the resonant process of nuclear excitation by electron capture (NEEC), an electron recombines into an atomic shell vacancy of an ion accompanied by the simultaneous excitation of the nucleus [171,172]. NEEC can occur when the initial (precapture) kinetic energy of the electron plus the electron binding energy released upon its capture matches the energy difference between the two nuclear states. For capture of a free electron, this mechanism, as originally conceived in 1976 by Goldanskii and Namiot [171], is the inverse of the internal conversion (IC) process discovered about 100 years ago and was correspondingly dubbed inverse internal electron conversion (IIEC). Only excitations from the nuclear ground state were treated in [171]. In 1989, Cue, Poizat, and Remillieux considered a similar scenario, but with the excitation of the nucleus of a projectile ion arising from capture of a target-bound electron; they coined the term NEEC [173] which, in later theoretical developments (see [174,175]) replaced the name IIEC for free-electron capture as well. Zadernovsky and Carroll later extended the NEEC concept to excitations from a nuclear isomer, rather than the ground state, as a mechanism for isomer depletion [176]. Very recently Carroll and Chiara published a review article on isomer depletion [177]. NEEC has been investigated theoretically or envisaged experimentally in channeling through crystals, laser-generated or astrophysical-type plasmas, storage rings, or electron beam ion traps (EBITs). NEEC with reshaping of electron wave functions or with excited ions has also been studied theoretically. Related references can be found in [178]. In the context of $^{229}$Th, NEEC was investigated theoretically for the scenario of a direct excitation to the isomer $^{229m}$Th in a plasma generated in a laser-cluster interaction [179]. Moreover, an efficient production of the nuclear clock isomer $^{229m}$Th through excitation of $^{229}$Th to its second excited state at 29.19 keV via NEEC was theoretically studied in [178]. In general, the discussion of the NEEC process is closely related to the question of depleting long-lived nuclear isomers, as long-lived nuclear metastable states can store large amounts of energy over long periods of time. Provided a suitable nuclear level scheme, an excitation, possibly via the atomic shell, can proceed from the isomeric state to a higher-lying gateway level. Then, the

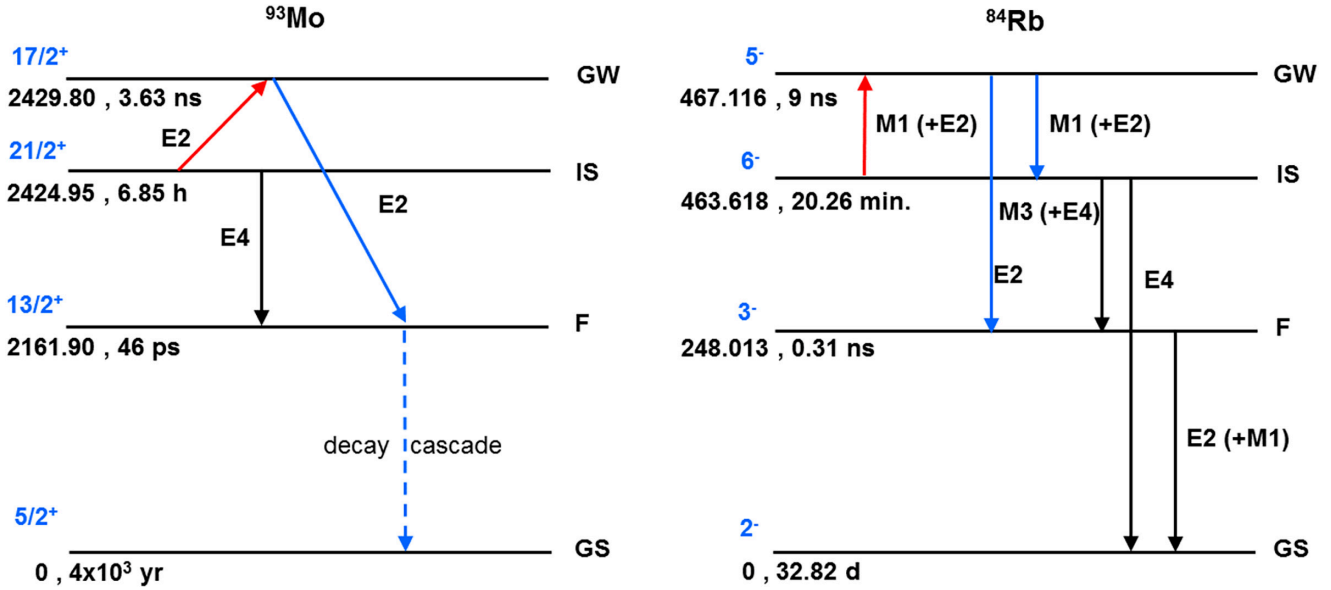


FIG. 5. Left: Illustration of the isomer depletion in $^{93m}$Mo following (e.g., NEEC induced) excitation of the isomer (IS) into a higher-lying gateway state (GW), followed by a rapid E2 decay cascade (F) towards the ground state (GS). Right: level scheme with isomer depletion scheme for $^{84m}$Rb.

subsequent nuclear decay may proceed directly to a state below the isomer, thus allowing to reach the ground state in a fast cascade. Such a decay sequence is called isomer depletion, as it allows for the depopulation of the isomeric state and thus a controlled release of the energy stored in the long-lived metastable state. Isomer depletion has been discussed as a potential energy storage solution (nuclear battery). Figure 5 (left panel) exemplifies the described scenario for the prototypical example of the long-lived (t1/2= 6.85 h) $I^{\pi} = 21/2^{+}$ isomer at an excitation energy of about 2.42 MeV in $^{93}$Mo. Due to the large spin difference, the (E4) decay of the isomer to the lower adjacent nuclear level (F, $I^{\pi} = 13/2^{+}$) is strongly hindered, however, if an E2 excitation into the upper $I^{\pi} = 17/2^{+}$ level could be achieved, e.g., via NEEC, then a rapid depopulation via a cascade of fast E2 transitions would be initiated. A comparable scheme holds for $^{84}$Rb, as shown in the right panel of Fig. 5. The NEEC process for the $^{84m}$Rb isomer ($I^{\pi} = 6^{-}$, $t_{1/2} = 20.26$ min) allows for an excitation by magnetic-dipole (M1) and electric-quadrupole (E2) transitions into a depletion gateway level ($I^{\pi} = 5^{-}$), which subsequently decays, releasing a substantial amount of stored energy [180].The first claim of experimental observation for NEEC was reported 2018 through $^{93m}$Mo isomer depletion in a beam-based fusion-evaporation scenario [181]. However, subsequent theoretical calculations contradict the experimental value for the NEEC excitation probability as being orders of magnitude higher than theoretical expectations [182–184], and the subject remains since then controversially debated [185,186]. A new and similar experiment has been performed with an isomer beam, but no signal of isomer depletion was observed [187]. Moreover, in the beam-based theoretical study of [180] the total NEEC probability (M1 plus E2) for the $^{84m}$Rb isomer is found to be almost three orders of magnitude higher than that predicted for the $^{93m}$Mo isomer. This makes the $^{84m}$Rb isomer a promising candidate for new NEEC beam-based experiments. Also, in [178] it could be shown that the production rate of $^{229m}$Th per nucleus via NEEC with presently accessible experimental conditions can be six orders of magnitude larger than the value experimentally demonstrated using 29-keV synchrotron radiation for this indirect excitation scheme. With an efficient production of $^{229m}$Th, a scenario has been identified with which NEEC events could be identified, for a clear experimental identification of the long-sought NEEC phenomenon.

### D. Nuclear excitation by electronic transition (NEET)

The excitation of nuclear levels induced by the transfer of energy from the atomic part to the nuclear part of an atom has been the subject of a large number of investigations. The aim underlying this research is the possibility of finding an efficient mechanism to excite nuclear isomers in view of further applications for energy storage and the development of lasers based on nuclear transitions. Nuclear excitation by electronic transition (NEET) is a rare decay mode for excited atomic states resulting in nuclear excitation [187]. Atomic states normally decay via x-ray emission and/or Auger electron emission. Exchange of a virtual photon induces NEET as a second-order effect. Hence, the NEET probability is small, many orders of magnitude less than atomic deexcitation by x-ray emission. NEET requirements include an energy degeneracy between the atomic and nuclear states, and the same transition multipolarity between the states. NEET was first discussed by Morita in 1973 to explain the excitation of a level at approximately 43 keV in $^{235}$U [188]. The idea was later applied to the excitation of other low-energy levels in a variety of nuclei. The best known low-energy transitions that have been considered are the transitions at 77.3, 69.5, and 102.9 keV, respectively, in the nuclei $^{197}$Au [189], $^{189}$Os [190], and $^{237}$Np [191]. However, initially contradictory results were obtained for the NEET process probability in these nuclei [192,193]. The development of intense beams of synchrotron radiation

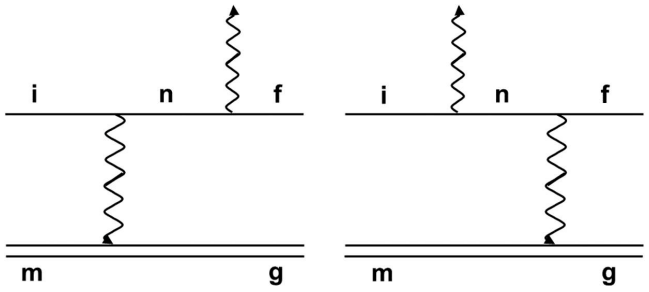


FIG. 6. Feynman diagrams of the electronic bridge (EB) process. The single and double solid lines relate to the electronic (*i*: initial, *n*: intermediate, *f*: final state) and the nuclear transitions (*m*: excited isomeric, *g*: ground state), respectively. The dashed lines are the photon lines. Adapted from [131].

has enabled experiments designed to determine the probability of NEET induced by synchrotron radiation in nuclei where the NEET conditions are met. Experimental observation of NEET induced by synchrotron radiation has been reported by Kishimoto *et al*. in $^{197}$Au [189]. The excitation probability for NEET of the level at 77 keV in $^{197}$Au was deduced as $(5.0 \pm 0.6) \times 10^{-8}$, by about a factor of 2 in agreement with the theoretical prediction in [194]. Various experimental attempts to identify NEET in $^{235}$U and determine its excitation probability via the (laser-generated plasma induced) excitation of the 26-min isomer $^{235m}$U remained unsuccessful so far [195,196]. Moreover, NEET has also been discussed theoretically as a new and effective way to populate the thorium isomer $^{229m}$Th [197].

### E. Electronic bridge

Lastly, the electronic bridge (EB) will be discussed as another scenario capable of nuclear excitation involving the atomic shell as mediator, specifically targeting the nuclear clock isomer $^{229m}$Th. The enhancement of $\gamma$-decay rates through the excitation of shell electrons to higher-lying bound states has been the subject of extensive theoretical studies, and the term "electronic bridge" (EB) was introduced in this context [198]. The inverse process is the previously discussed process of nuclear excitation by electron transition (NEET). The EB is a process coupling a nuclear transition to an electron transition in the atomic shell via electromagnetic interactions. This mechanism becomes relevant especially in the case of low-energy transitions, where the radiation wavelength exceeds the nuclear size by many orders of magnitude and radiative coupling to the larger electron shell serves as a somewhat better matched antenna [9]. Fortunately, the EB does not require a perfect energetic match between the atomic and nuclear transitions: the energy mismatch is covered by the emission or absorption of a photon. This process was first investigated theoretically in [199,200] for resonant processes, later extended in [198] also to nonresonant processes. In the literature the term EB is used both for nuclear excitation and for nuclear decay, with the corresponding atomic shell transitions. The EB process can be illustrated by the two Feynman diagrams displayed in Fig. 6. In the following we assume that the initial $i$ and the final $f$ electronic states are of opposite parity and fixed. A real electric dipole photon is emitted or absorbed. The EB process can be effectively treated as the electric dipole $i \rightarrow f$ transition of the electron accompanied by the nuclear transition from its isomeric state $m$ to the ground state $g$. First experimental observation of nuclear deexcitation via an electronic-bridge mechanism was reported through studying the deexcitation of the 30.7-keV ($t_{1/2}$ Ĩ3.6 yr) isomeric level of $^{93}$Nb with the electronic bridge involving initial-state *L*-shell electrons and final-state *N*-shell or higher electrons [201]. Agreement within a factor of 4 was achieved with theoretical calculations [202]. To date, EB schemes for nuclear excitation in $^{229}$Th have been theoretically investigated for $^{229}$Th [121,203], $^{229g}$Th$^{+}$ [131,132], $^{229}$Th 2+ [8], $^{229}$Th$^{3+}$ [133,204–207], $^{229}$Th$^{35+}$ [135], and $^{229}$Th-doped ($CaF_2$) crystals [136]. Specifically, triply charged $^{229m}$Th ions are favorable to be stored in an ion trap for laser manipulations. Owing to their simple electronic energy levels (one valence electron outside an inert Rn core), the trapped $^{229}$Th$^{3+}$ ions can be laser cooled to form a linear-chain Coulomb crystal using two closed transitions in the nuclear ground state of $^{229}$Th$^{3+}$ ($^{229g}$Th$^{3+}$) [208]. When the Th ions are prepared in the $7P_{1/2}$ state, EB excitation can be triggered by a 350-nm laser, and isomeric states are expected to be populated. Finally, the isomeric state is detected based on the isomer shift of the cooling lasers [115].

## IV. ELECTRON PROCESSES IN ATOMIC AND MOLECULAR PHYSICS

In this section we review electronic processes relevant in atomic and molecular physics. Particular emphasis is given to the time-resolved techniques that enable access to the light-induced electron dynamics at its intrinsic timescale. A specific focus is given to photoemission and the ability to reveal electron correlation effects via attosecond time-resolved photoemission delays. Additionally, molecular processes resulting from the electron-electron or electron-nuclei interactions such as charge migration and charge transfer are discussed. We make an important note concerning formalism: in this section, electron-nuclei interactions refer to nonadiabatic processes in molecular physics, i.e., the coupling between electronic states and the movement of atoms within a molecule. In the other sections, electron-nucleus couplings refer instead to the interaction between electrons and nuclear states.

### A. Photoemission delays and electron-electron interactions

The photoelectric effect, which leads to the emission of an electron from a target when exposed to a photon with energy exceeding the binding energy, is well understood. However, for long it has been debated whether the emitted electron appears in the continuum instantaneously or with a brief delay. When treated from a quantum mechanical perspective, it becomes evident that photoemission must occur with a certain delay. Indeed, the photoemission process can be accurately described as a half-scattering mechanism involving the outgoing electron wave packet (EWP) interacting with the binding potential. Reviving the quantum scattering theory proposed by Eisenbud [209] and Wigner [210] first and later by

Smith [211], it is indeed possible to extract a scattering delay. Specifically, the scattered electronic wave experiences a phase shift relative to a wave propagating in a potential-free region. This phase shift is referred to as the Eisenbud-Wigner-Smith (EWS) phase, and its energy derivative corresponds to a finite delay known as the EWS delay. Since in the photoemission process the EWS delay typically ranges from a few tens of attoseconds to hundreds of attoseconds, the direct measurement of this delay has remained inaccessible until attosecond light sources became available.

As outlined in Sec. II, attosecond pulse generation relies on a strong-field mechanism known as high-order harmonic generation (HHG) [74–76]. HHG produces a frequency comb consisting of odd-order harmonics of the driving laser frequency, which corresponds to a train of attosecond pulses in the time domain. By using gating techniques, a single attosecond pulse can be isolated, leading to continuous emission across several tens or hundreds of eV within the extreme ultraviolet (XUV) and soft x-ray spectral ranges, respectively. The timing of the photoemission process can be achieved through two main pump-probe approaches: The first one is named RABBITT (reconstruction of attosecond beating by interference of two-photon transitions) [212], while the second one is named attosecond streak camera [213,214]. A comprehensive review of the measurement of photoemission delays using both approaches can be found here [215].

In both RABBITT and streaking, a target is photoionized in the copresence of XUV and near-infrared (NIR) laser pulses that are phase locked. The resulting photoelectrons are collected as a function of the delay between the two pulses (similarly to the pump-probe concept explained in previous sections). In RABBITT, an attosecond pulse train is used, where quantum interference between two ionization pathways that lead to the same final photoelectron energy is used to determine the phase of the EWP. In the attosecond streak camera technique, an isolated attosecond pulse is employed, and the NIR field modulates the momentum of the photoemitted EWP. The NIR field acts as a phase gate in a time-resolved manner akin to frequency resolved optical gating (FROG) [216], which is used to retrieve the spectral phase of optical laser pulses. Generalized projection algorithms allow for the extraction of the phase of the photoemitted EWP from the streaking spectrogram [217].

In attosecond time-resolved measurements, the extracted EWP phase includes two additional contributions to the EWS phase ($\Delta\phi_{\mathrm{EWS}}$) that must be taken into account: The first one, $\Delta\phi_{\mathrm{XUV}}$, commonly referred to as the attochirp [218,219], originates from the spectral phase of the ionizing attosecond pulse (or attosecond pulse train). The second contribution, $\Delta\phi_{\mathrm{CC}}$, originates from the so-called continuum-continuum transitions, which are mediated by the NIR probe pulse in the tail of the Coulombic potential [220,221]. Several theoretical and experimental works reported on the precision with which the two above-mentioned approaches allow the extraction of $\Delta\phi_{\mathrm{EWS}}$, and consequently the EWS delay, for several atomic [220,222–226] and molecular species [227–232]. It is important to note that molecular photoionization presents additional complexities compared to the atomic case. Specifically, it has been shown that photoemission delays depend on both the molecular orientation and the multicenter character of the Coulombic potential. Furthermore, it has been demonstrated that nuclear motion in molecules significantly influences the photoemission time extracted from both RABBITT and streaking techniques [233]. Photoemission delays have been measured across a broad range of targets, including rare gas atoms, increasingly complex molecules [234], liquids [235], and solids [236–239]. The information carried by the measured attosecond photoemission delays varies according to the type of system under investigation. In the gas phase, these delays typically reflect the scattering of electrons within the Coulombic potential. In contrast, in the liquid or solid state, they generally provide insights into the transport dynamics towards the surface.

Beyond facilitating the precise determination of the phase shifts induced by the Coulombic potential and the laser field, the EWS phase also carries significant information about electron-electron interactions. Specifically, in the proximity of resonances, the correlated dynamics of the photoionized resonant EWP strongly affects the photoemission delay. In this context, extensive studies have been conducted in the proximity of autoionizing resonances, where electron correlation effects dominate the dynamics. In noble gases, the typical signature of these autoionizing resonances is an asymmetric line shape in the absorption spectrum, which has been explained by Fano in the framework of the configuration interaction (CI) as an interference effect between the direct photoionization channel and an indirect channel resulting from the photoexcitation of an electron to a bound state embedded in the ionization continuum [240,241]. These bound states are short lived and decay via the autoionization process into continuum states. Signatures of these autoionizing resonances have been found, experimentally and theoretically, in the photoemission delays extracted from atomic species both with RABBITT [242,243] and streaking [244,245] approaches. Using a spectrally resolved RABBITT approach (Rainbow RABBITT), it has been possible to follow the building up of a Fano resonance on a sub-fs timescale [246].

In the context of photoionization and electron correlation effects, it is worth mentioning the peculiar case of subnanometer plasmonic systems such as fullerenes. Fullerenes are cage-shaped single molecules of $n$ carbon atoms (Cn), with C60 being the most extensively studied [247]. Due to the highly delocalized nature of their valence molecular orbitals surrounding the carbon cage, fullerenes exhibit distinctive giant plasmonic resonances (GPRs) [248], which are collective electronic excitations occurring in the extreme-ultraviolet energy range. The ultrabroadband nature of these resonances suggests that they have intrinsically ultrashort lifetimes. When a GPR is excited, photoionization takes place, and the scattering of the outgoing electron wave packet on the plasmonic potential provides crucial information about the nature of the resonance. Recent attosecond time-resolved streaking measurements in C60 have uncovered the quantum nature of these GPRs, revealing a strong role of electron correlation effects [249]. These findings indicate that to accurately describe plasmon dynamics in subnanometer particles, it is essential to move beyond the classical model of collective single-particle electron motion and properly account for electron-electron interactions.

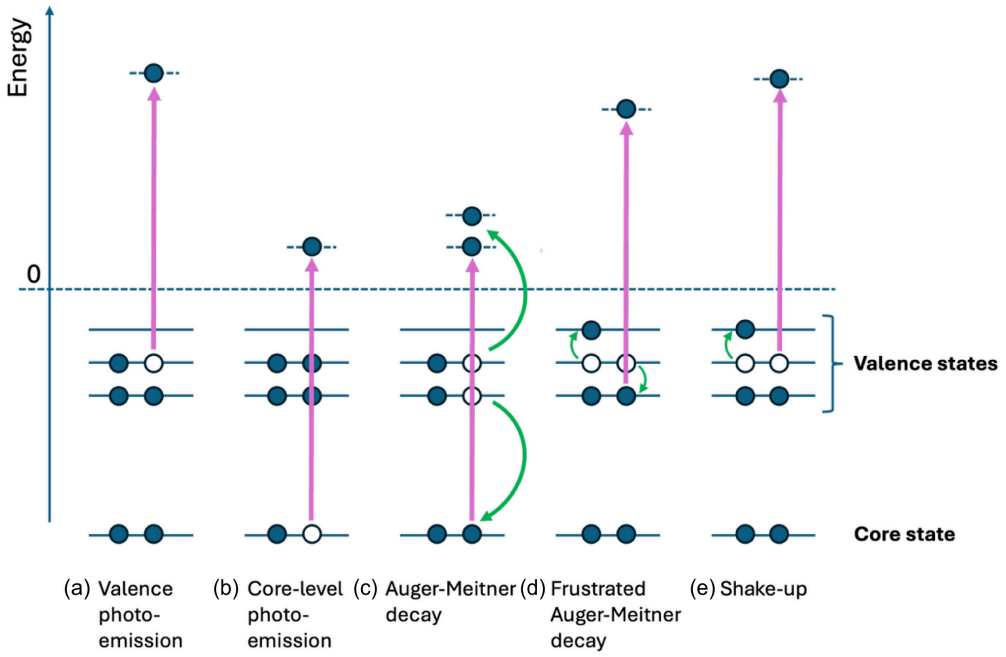


FIG. 7. Schematic of the photoemission process from valence or core levels: Possible electronic reorganization processes, following the creation of the hole, are also shown. Purple arrows indicate the bound-continuum transitions induced by the absorption of one XUV photon from a valence (a) or a core state (b). Green arrows indicate the internal electronic reorganizations occurring during different scenarios: Auger-Meitner decay [(c), following (b)], frustrated Auger-Meitner decay [(d), following (a)] and shakeup [(e), following (a)]. The Auger-Meitner process is the only one resulting in the creation of two free charges: the photoelectron and the Auger electron.

### B. Charge migration and charge transfer

Electron-electron interactions play a central role when electrons are photoionized from inner valence or core states in atoms and molecules. The creation of a hole inevitably leads to a rearrangement of the electronic system, giving rise to radiative and/or nonradiative recombination. Among the various relaxation mechanisms, the most common are the Auger-Meitner decay and shakeup processes. As shown in Fig. 7, the Auger-Meitner (shakeup) is a multielectron process in which the hole created by photoionization is filled by one electron from a valence orbital, while the excess of energy is ceased to a second electron that is emitted (excited to outer valence). These relaxation mechanisms generally occur on ultrafast timescales, ranging from subfemtoseconds to a few femtoseconds and have been followed in real time for instance by employing the streaking approach described above [250,251]. More recently, the coherent electronic motion initiated by x-ray core photoionization of a small molecule and the subsequent Auger-Meitner decay have been resolved by using angular streaking and attosecond free-electron laser pulses [252].In addition to hole recombination, molecules exhibit another fascinating mechanism known as charge migration [253]. This process involves the movement of a hole along the molecular backbone. Studies have shown that during charge migration, charge fluctuations can occur at nearly all molecular sites, without a distinct preference for specific functional groups [76]. This phenomenon challenges traditional chemical assumptions, revealing that functional groups with high electron affinity might temporarily possess less electronic charge compared to those with lower or negligible electron affinity, albeit for just a few hundred attoseconds. Such behavior can cause significant yet temporary changes in chemical bonding. This area of study has garnered significant interest due to its potential to facilitate new strategies for controlling chemical reactions by manipulating charge motion.

In a frozen nuclei configuration, the charge exhibits back-and-forth oscillations, with a periodicity solely determined by the energy difference between the electronic states involved in the ionization process. This period typically ranges from a few femtoseconds down to several hundreds of attoseconds. However, in practice, the onset of the nuclear motion can induce decoherence, interrupting the charge migration, and cannot be neglected when modeling the process [254–258]. Charge migration was at first only theoretically predicted under the assumption of a "sudden ionization" event, causing the instantaneous removal of one electron from a highly correlated inner valence electronic state of the $C_3H_2F_2O$ (difluoropropadienone) molecule [253] and it was later computed for a large variety of molecules [259–261]. The formed electron wave packet was freely propagated in the basis of cation eigenstates at a fixed nuclear configuration. The first experiments on charge migration were instead performed in very different conditions: an attosecond XUV pump pulse was used to sudden ionize the molecular system (the amino acid phenylalanine) and a few-femtosecond NIR probe pulse was used to probe the XUV-induced charge migration by inducing photofragmentation at variable time delays. A fast modulation in the immonium dication yield was used to detect the typical oscillatory dynamics peculiar of the charge migration. This modulation was attributed to the periodic migration of

the hole between the amino and the carboxyl group of the molecule [262]. Given the broadband nature of attosecond light pulses, charge migration was in this case due to the coherent superposition of a manifold of electronic states that is inevitably created in the ionization step. Subsequently, a similar migration was found to occur in the suddenly ionized amino acid tryptophan [263]. The effect of the nuclear motion on the temporal evolution of this coherence was the subject of later studies.

The first experimental demonstration that charge migration can indeed be triggered by electron correlation effects has been achieved in the DNA base adenine [264,265]. Here, a shakeup mechanism, triggered by the sudden ionization of an inner valence state of adenine, has been identified as the mechanism behind the out-of-plane charge migration that occurs within a few femtoseconds. This charge redistribution enhances the likelihood of absorbing a second near-infrared (NIR) probe pulse, which subsequently leads the molecule into a doubly charged metastable state. Therefore, it has been concluded that in this context, charge migration facilitates an ultrafast stabilization mechanism that protects the molecule against dissociation.

Charge migration has been extensively studied using various methods, including time-resolved photoion [263,264] and photoelectron [266] spectroscopies, high-harmonic generation (HHG) based spectroscopy [267], and transient absorption spectroscopy [268]. Recently, research has shifted towards examining charge migration triggered by nonionizing radiation, such as ultraviolet (UV) light, in neutral molecules. Notably, recent studies have focused on UV-excited chiral molecules. Chiral molecules are nonsuperimposable mirror images of each other, known as enantiomers, and possess distinct chemical properties. As a result, molecular chirality is crucial in various applications, including bioresponsive imaging, molecular spintronics, and pharmaceuticals. When charge migration is initiated in a chiral molecule, it can create chiral currents. These currents serve as a highly sensitive chiroptical tool for enantiomeric discrimination and can induce dynamic changes in the chiral system's properties. Recent demonstrations of chiral currents and the ability to modulate the chiral optical response by activating charge migration in the molecule methyl lactate have opened new opportunities for controlling the enantioselective reactivity at ultrafast timescales [269].

Charge migration is a purely electronic mechanism inherently related to electron-electron interactions. However, it is important to note that charge dynamics can also be influenced by interactions between electrons and nuclei. This last case is known as charge transfer [270], and it has been the subject of extensive research for several decades due to its critical role in various photoinduced processes within chemically and biologically relevant systems, as well as in materials science. Charge transfer serves as a fundamental mechanism in numerous applications, including redox reactions, photovoltaics, and photocatalytic processes [1–3]. While charge migration occurs periodically, charge transfer is characterized by a one-way flow of charge from a donor to an acceptor site. This transfer can occur within a single molecule (intramolecular charge transfer) or between different molecules (intermolecular charge transfer). Furthermore, charge transfer can take place in various contexts, such as between a molecule and its solvent, between a metal and a ligand, or among different nanostructures and molecular complexes.

Charge migration typically occurs on the electron timescale (attoseconds to a few femtoseconds), while charge transfer can happen over much longer timescales, ranging from tens of femtoseconds to nanoseconds. As mentioned, charge transfer is often mediated by electron-nuclei interactions, particularly when different electronic states approach each other in energy and change character along specific nuclear coordinates.

It is important to note that there is no sharp boundary between charge migration and charge transfer; the influence of electronic coherence on subsequent charge transfer, once the nuclei begin to move, is still an area of active investigation. Exciting prospects for controlling chemical reactions arise from the potential to drive them along unconventional pathways through the coupling of electronic and vibrational coherences, a territory yet to be fully explored.

## V. TOWARD THE TIME-RESOLVED SPECTROSCOPY OF ELECTRON PROCESSES IN NUCLEAR TRANSITIONS

Until now, we have discussed the correlation between electronic and nuclear states and current opportunities to drive nuclear transitions through light. In this context, enhancing experimental capabilities to study the coupling between electrons and nuclei is an exciting prospect. Many studies suggest that electron channels, particularly when employing photoinduced schemes, offer opportunities to enhance or control the population of nuclear states [135,136,172,271–280]. However, intensive research is still needed to better understand the fundamental mechanisms governing this many-body problem, i.e., nucleus-electron-photon interactions, and the corresponding field of photoelectron spectroscopy remains largely unexplored. In particular, it is worth considering both the opportunities and limitations of applying time-resolved schemes, successfully employed in other branches of physics (see Sec. IV), to the problem discussed here. This section aims to outline the key aspects to be considered in the pursuit of establishing time-resolved spectroscopy for photoinduced electron dynamics in nuclear transitions.

### A. Conversion electron Mössbauer spectroscopy

Historically, spectroscopy of electron channels in nuclear transitions has primarily been conducted using conversion electron Mössbauer spectroscopy (CEMS) [276,277,281–283]. In the seminal works by Bonchev *et al.* [281] and Swanson and Spijkerman [282], electrons produced through internal conversion in Mössbauer isotopes were measured to characterize sample surfaces. Measuring conversion electrons offers several advantages over competing radiative channels: (i) Electrons rapidly lose kinetic energy when traveling through matter, meaning only those produced near the surface can escape from the bulk. For example, in the case of 7.3-keV $K$-conversion electrons in $^{57}$Fe, the penetration depth is less than 300 nm, with energy loss within the first 5 nm considered negligible [284–286]. (ii) They can be

detected with high efficiency and distinguished from photons. CEMS has become a standard method in materials science and physical chemistry for studying surface and interface processes, including corrosion [287–297], surface finishing [298–307], metal alloy formation [308–313], and thin-film oxidation [314–324], among many others [277]. The vast majority of CEMS experiments have been performed by driving the resonant excitation of Mössbauer isotopes using a radioactive sample as a gamma-ray source. For example, $^{57}$Co decays into $^{57}$Fe, emitting photons at 14.4 keV, which can then be used to resonantly excite the Mössbauer transition of $^{57}$Fe atoms in the sample under study, with the resulting ejected conversion electrons being detected [276,277,283]. With the advent of bright synchrotrons and free-electron lasers over the past two decades, it has become possible to drive Mössbauer transitions using external light sources, expanding Mössbauer spectroscopy into a new range of studies [49,56,57,111,152,153,325–329]. However, most of these studies have focused on radiative channels, and the application of CEMS at large-scale facilities has remained largely unexplored. One of the few examples available in the literature is the work by Sturhahn *et al.* [46], which investigated time-dependent electron emission from iron foils excited by synchrotron radiation at the 14.4-keV nuclear resonance of $^{57}$Fe. Their study focused on incoherent nuclear resonant scattering (NRS) [49], examining the energy exchange between nuclear states and phonon modes activated in the surrounding material. Utilizing a high-resolution monochromator and an electron detector with microchannel plates (MCPs), the experiment identified three key emission mechanisms: conversion electron emission with and without phonon interactions and photoelectron emission. The results showed that thin iron layers exhibited natural decay, whereas thicker foils demonstrated quantum beats indicative of coherent elastic NRS. The emission behavior was influenced by foil thickness, with conversion electrons dominating in thinner layers and photoelectrons becoming more significant as thickness increased. Additionally, the study examined phonon-mediated processes, which, though less prominent due to interference from *K*-fluorescence radiation, provided valuable insights into lattice vibrations and nuclear interactions. To interpret the experimental data, a theoretical model based on quantum electrodynamics was developed, incorporating virtual photon exchange between excited nuclei and the electron shell. This model successfully captured the observed decay patterns and time-dependent variations in electron emission, providing a quantitative framework for analyzing nuclear excitation processes. The findings of Sturhahn and coworkers underscored the significance of both coherent and incoherent NRS in modifying electron emission characteristics, highlighting potential applications of these mechanisms in advanced spectroscopic techniques. Furthermore, the study demonstrated how synchrotron radiation can be used to probe nuclear dynamics at highly localized scales, with implications for fields such as condensed matter physics and materials science. This example of CEMS has led to a deeper understanding of the interplay between nuclear resonance phenomena and electronic excitations. In general, promising new perspectives can arise from combining modern light sources with conversion electron spectroscopy. When an internal conversion electron is ejected from a core atomic shell, as in the case of $^{57}$Fe, the process is typically followed by secondary processes, including the emission of Auger electrons. By resolving the kinetic energy of this broad spectrum of electron channels, it may be possible not only to extract depth-dependent escape information, as demonstrated in [46], but also to gain deeper insights into the complex energy exchange between the nuclear state and its surrounding environment. While these questions have already been explored in traditional CEMS studies, the use of novel light sources could be a game changer. By optically perturbing electronic degrees of freedom, new schemes could emerge where such perturbations act as precise probes or control mechanisms for nuclear transitions.

### B. Electron-nucleus coupling upon optical perturbation

The role of electron processes in nuclear transitions accompanied by photoexcitation has gained attention due to its potential for enhancing and controlling the population of nuclear states [120,197,206,330–334]. As one example, Nickerson *et al.* [136] explored the excitation of the $^{229}$Th isomer in doped $CaF_2$ crystals, introducing a more efficient approach based on electronic bridge (EB) mechanisms. In their study, the authors demonstrated that thorium doping in $CaF_2$ creates defect states within the crystal's band gap. Rather than being a hindrance, these defect states can facilitate nuclear excitation by enabling energy transfer to the nuclear isomer through EB processes, which involve stimulated emission or absorption via optical lasers. Their results show that EB excitation rates are at least two orders of magnitude higher than those of direct photoexcitation, making this method significantly more effective. Using density functional theory (DFT), the study analyzed the interaction between defect states and the $^{229m}$Th isomer, considering both spontaneous and laser-assisted EB processes. The efficiency of these mechanisms depends on the alignment of defect states with the isomer's transition energy. Additionally, the authors found that reverse EB mechanisms can quench the isomeric population, leading to a rapid, controlled decay and producing a signal three orders of magnitude stronger than natural radiative decay. The high flux and tunability of modern optical lasers open new avenues for studying nuclear state relaxation following the photoexcitation of specific electronic states. This concept is illustrated in Fig. 8, which depicts the internal conversion (IC) process following nuclear state excitation (see Sec. III for a detailed explanation of IC). This scenario is particularly relevant to the relaxation of the isomeric transition in $^{229}$Th, which we use here as an example. The first excited state of $^{229}$Th ($|e\rangle_n$) can be populated either through direct photoexcitation with VUV light [23,25] or via the decay of $^{233}$U [58]. In neutral $^{229}$Th atoms, the excited nuclear state primarily relaxes to the ground state ($|g\rangle_n$) through internal conversion, transferring energy to the surrounding electron shell. The nucleus efficiently couples to the highest occupied electronic state in the valence band ($|i_0\rangle_e$), leading to electron emission [IC emission, Fig. 8(a)]. It is important to note that the schematic representation in Fig. 8(a) is simplified. In all currently available experimental implementations [23,25,58,69], IC emission is never measured from isolated $^{229}$Th atoms. Instead, $^{229}$Th states are hybridized by their surrounding environment, such as the

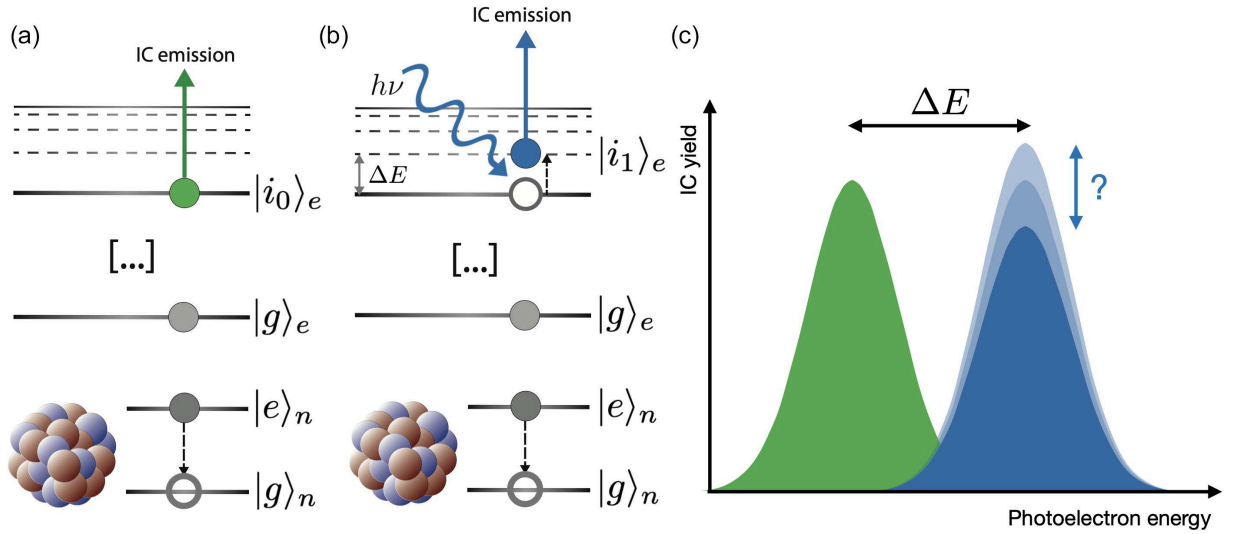


FIG. 8. Sketch of internal conversion upon the photoexcitation of an electronic state. This case applies to the IC relaxation of the $^{229m}$Th isomer. (a) IC without optical perturbation. The excited nuclear state $|e\rangle_n$ relaxes into the ground state $|g\rangle_n$ by triggering IC in a valence electron state ($|i_0\rangle_e$). Intermediate (core and inner valence) states are omitted in the sketch for simplicity. (b) IC with optical perturbation. An external optical source triggers population transfer from $|i_0\rangle_e$ to the lowest unoccupied state $|i_1\rangle_e$. (c) Sketch of the IC electron energy distribution, with the possible outcome of the IC yield from $|i_1\rangle_e$.

graphene foils used for $^{229}$Th ion neutralization [69]. Consequently, the emitted photoelectron wave packet exhibits a central energy and bandwidth that depend on the experimental conditions. In Fig. 8(b), IC emission is influenced by the presence of electromagnetic radiation, such as a continuous-wave laser, with photon energy $h\nu$. If $h\nu$ is resonant with the transition between the highest occupied electronic state ($|i_0\rangle_e$) and the lowest unoccupied state ($|i_1\rangle_e$), population transfer occurs from the former to the latter. This perturbation not only alters the electronic configuration of the atom but also affects nucleus-electron coupling and the IC process. By analyzing the IC emission yield from the photoexcited state [Fig. 8(c)], one can determine whether the IC mechanism via $|i_1\rangle_e$ is facilitated or suppressed. More generally, such investigations enhance our understanding of energy transfer between nuclear states and the surrounding atomic shells. This would also serve as a fundamental demonstration of photocontrolled nucleus-electron coupling.

### C. Perspectives for time-domain studies of electron-nucleus couplings

In the previous paragraph, we discussed several examples of controlling electron-nucleus coupling through light; however, the discussion was limited to static perturbations, such as the scenario depicted in Fig. 8(b). Drawing a parallel with electron dynamics in atomic and molecular physics (see Sec. IV), we now extend our discussion to address the following open questions:

(i) Can we track the energy exchange between a nuclear state and the surrounding electronic degrees of freedom in real time?

(ii) Can we establish protocols for the time-resolved study of electron processes in nuclear transitions?

Tackling these challenges first requires a clear understanding of the relevant timescales in electron-nucleus couplings. As discussed in Sec. IV, while the intrinsic timescale of electron motion ranges from a few femtoseconds to attoseconds, electron dynamics in matter can evolve over much longer characteristic times when coupled to other degrees of freedom, as seen in nonadiabatic processes. In nuclear physics, nuclear state decays occur over an extraordinarily broad range of timescales. Unstable nuclei at the boundary of the drip line can show decay times shorter than $10^{-18}$ s [335–337], whereas the isomeric transition in $^{229}$Th ions has a radiative decay time of approximately $10^3$ s [23,25]. However, when the same transition in $^{229}$Th decays via internal conversion (IC), the decay time is significantly shorter, on the order of microseconds (see Sec. III). This is because coupling with electronic degrees of freedom typically broadens the natural linewidth of the nuclear transition, leading to a reduced decay time. In this context, the example presented in Fig. 8 already provides an interesting perspective for time-resolved studies. By photoexciting $|i_1\rangle_e$, the density of states involved in the IC process may change compared to the unperturbed case, potentially altering the IC decay time. Given the extremely narrow linewidth and long decay time of the isomeric transition in $^{229}$Th, even when broadened through IC, we do not discuss the application of pump-probe schemes here. For nuclear states with higher transition energies, such as those in $^{57}$Fe and $^{45}$Sc, the scenario becomes even more complex. In $^{57}$Fe, the Mössbauer transition has a decay time of 142 ns [49] and efficiently couples to the $K$ and $L$ shells through IC. IC emission from core states initiates an ultrafast cascade of secondary processes, including Auger emission [277]. Additionally, phonon modes in the material are typically activated in correlation with the Mössbauer effect, and these have been investigated using nuclear inelastic scattering [325,338–340]. From this analysis, it is evident that a rich ensemble of interactions exists between the nucleus and its surrounding degrees of freedom. Exploring these interactions in a time-resolved manner could significantly advance our

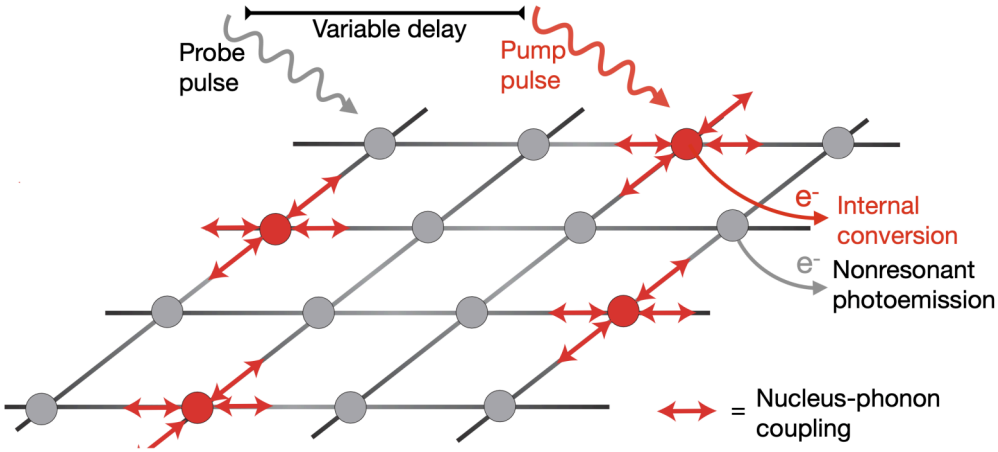


FIG. 9. Schematic representation of a possible pump-probe time-resolved study of the energy exchange between nuclei, electronic states, and phonons upon Mössbauer resonant excitation in lattice.

understanding of nuclear-electronic coupling dynamics. To the best of our knowledge, no time-resolved study has yet been reported that directly tracks, in real time, the energy exchange between nuclear states and phonons within the framework of Mössbauer spectroscopy. However, recent advancements in the photoexcitation of Mössbauer transitions using FEL pulses have paved the way for an entirely new class of experiments, potentially enabling pump-probe studies. Figure 9 presents a sketch of a possible experimental scheme. A pump pulse is used to resonantly excite a nuclear transition, while a probe pulse is tuned to a specific atomic shell. By varying the delay between the pump and probe pulses, time-resolved measurements of internal conversion and direct photoelectron emission could provide valuable insights into the transient energy exchange between the nuclear state, surrounding atoms, and the lattice.

### D. The relevance of multidimensional observables

As discussed in the perspective examples provided in this section, investigating the time-resolved electron dynamics during nuclear transitions entails the intrinsic coexistence of multiple, temporally overlapping processes. When a nucleus is resonantly excited, a rich manifold of competing mechanisms unfolds alongside the relaxation pathways of the nuclear state itself. These include, for example, direct photoionization followed by Auger decay and secondary electron cascades, or slower processes such as electron-phonon coupling. This complexity leads to ambiguities in interpreting experimental observables, posing a challenge to selectively probing electron-nucleus dynamics in time-resolved experiments. A promising route to address this challenge lies in exploiting the full dimensionality of the measured observables. Inelastic nuclear resonant scattering techniques, for instance, offer energy selectivity by scanning the incident photon energy around the nuclear transition. When combined with energy-resolved photoelectron spectroscopy, these methods may enable clearer identification of electron dynamics following nuclear transitions, helping to disentangle resonant from nonresonant contributions. Furthermore, if not only the kinetic energy but also the momentum (or angular distribution) of the photoelectrons is resolved, this approach can help lift degeneracies, such as those between coherent and incoherent emission, associated with distinct intermediate or final states. Of particular interest is the time-of-flight (TOF) dimension, which serves as a selective observable owing to the characteristically long-lived nature of nuclear excitations: electrons emitted as a result of nuclear decay or internal conversion are temporally delayed relative to prompt photoelectrons and can thus be distinguished. These examples collectively suggest that the feasibility of investigating electron-nucleus couplings relies not only on tailored photoexcitation schemes but also on the multidimensional nature of the observables under study. Selectivity, in this context, emerges as a key requirement for advancing time-resolved spectroscopy of photoinduced electron dynamics in nuclear transitions.

## VI. CONCLUSIONS

The study of photoinduced nuclear transitions and related electron processes has garnered significant attention in recent years, with the potential to revolutionize multiple disciplines, including high-precision metrology and quantum technologies, while deepening our understanding of fundamental physics. Advancing our knowledge of electron-nucleus couplings and their dynamics plays a crucial role in this context. By leveraging recent advancements in light sources, such as free-electron lasers (FELs), synchrotrons, and table-top laser setups, researchers now have unprecedented opportunities to investigate nucleus-electron couplings with high precision and, potentially, in the time domain. In this work, we have provided a comprehensive overview of the fundamental mechanisms underlying these interactions, with a particular emphasis on advanced light sources and the possibility of developing time-resolved approaches. By addressing the challenges outlined in this study, researchers can establish new concepts in nuclear spectroscopy, where new avaiable photon sources and time-domain investigations offer unprecedented insights into the intricate interplay between nuclear and electronic states. As experimental capabilities continue to

advance, we may significantly enhance our understanding of nuclear processes by integrating insights from other branches of physics.

## ACKNOWLEDGMENTS

F.C. acknowledges financial support from the Cluster of Excellence "CUI: Advanced Imaging of Matter" of the Deutsche Forschungsgemeinschaft (DFG)-EXC 2056–Project No. 390715994, the German Research Foundation (DFG)—SFB-925—Project No. 170620586 and the Open Access Publication Fund of Universität Hamburg. P.G.T. acknowledges support via the "ThoriumNuclearClock" project that received funding from the European Research Council (ERC) under the European Union's Horizon 2020 Research and Innovation Programme (Grant Agreement No. 856415). A.T. acknowledges support from the Helmholtz Association under the Helmholtz Young Investigator Group VH-NG-1603, and financial support from the European Research Council under the ERC SoftMeter Grant No. 101076500. Views and opinions expressed are however those of the author(s) only and do not necessarily reflect those of the European Union or the European Research Council Executive Agency.

[1] D. Nolfi-Donegan, A. Braganza, and S. Shiva, Mitochondrial electron transport chain: Oxidative phosphorylation, oxidant production, and methods of measurement, Redox Biology **37**, 101674 (2020).
[2] C. C. Moser *et al.*, Nature of biological electron transfer, Nature (London) **355**, 796 (1992).
[3] R. Croce and H. van Amerongen, Natural strategies for photosynthetic light harvesting, Nat. Chem. Biol. **10**, 492 (2014).
[4] A. Aldahan *et al.*, Atmospheric impact on beryllium isotopes as solar activity proxy, Geophys. Res. Lett. **35**, 2008GL035189 (2008).
[5] M. Alotby *et al.*, Measurement of the intensity ratio of auger and conversion electrons for the electron capture decay of $^{125}$I, Phys. Med. Biol. **63**, 06NT04 (2018).
[6] M. Alotiby *et al.*, Quantitative electron spectroscopy of $^{125}$I over an extended energy range, J. Electron Spectrosc. Relat. Phenom. **232**, 73 (2019).
[7] J. Thielking *et al.*, Laser spectroscopic characterization of the nuclear-clock isomer $^{229m}$Th, Nature (London) **556**, 321 (2018).
[8] E. Peik and M. Okhapkin, Nuclear clocks based on resonant excitation of $\gamma$-transitions, C. R. Phys. **16**, 516 (2015).
[9] E. Peik *et al.*, Nuclear clocks for testing fundamental physics, Quantum Sci. Technol. **6**, 034002 (2021).
[10] K. Beeks *et al.*, The thorium-229 low-energy isomer and the nuclear clock, Nat. Rev. Phys. **3**, 238 (2021).
[11] N. Dimarcq *et al.*, Roadmap towards the redefinition of the second, Metrologia **61**, 012001 (2024).
[12] J. Kromdijk *et al.*, Improving photosynthesis and crop productivity by accelerating recovery from photoprotection, Science **354**, 857 (2016).
[13] M. Mitrano *et al.*, Possible light-induced superconductivity in $K_3C_{60}$ at high temperature, Nature (London) **530**, 461 (2016).
[14] A. Zong *et al.*, Emerging ultrafast techniques for studying quantum materials, Nat. Rev. Mater. **8**, 224 (2023).
[15] H.-T. Chen, A. J. Taylor, and N. Yu, A review of metasurfaces: Physics and applications, Rep. Prog. Phys. **79**, 076401 (2016).
[16] S. Matinyan, Lasers as a bridge between atomic and nuclear physics, Phys. Rep. **298**, 199 (1998).
[17] M. Maiuri, M. Garavelli, and G. Cerullo, Ultrafast spectroscopy: State of the art and open challenges, J. Am. Chem. Soc. **142**, 3 (2020).
[18] R. L. Mössbauer, Kernresonanzfluoreszenz von Gammastrahlung in Ir$^{191}$, Z. Phys. **151**, 124 (1958).
[19] P. P. Craig *et al.*, Nuclear resonance absorption of gamma rays in Ir$^{191}$, Phys. Rev. Lett. **3**, 221 (1959).
[20] S. I. Aksenov *et al.*, Observation of resonance absorption of gamma rays in zn67, Sov. Phys.–JETP **13**, 62 (1961).
[21] C. Alff and G. K. Wertheim, Hyperfine structure of Fe$^{57}$ in yttrium-iron garnet from the Mössbauer effect, Phys. Rev. **122**, 1414 (1961).
[22] W. Decking *et al.*, A MHz-repetition-rate hard x-ray free-electron laser driven by a superconducting linear accelerator, Nat. Photon. **14**, 391 (2020).
[23] J. Tiedau *et al.*, Laser excitation of the Th-229 nucleus, Phys. Rev. Lett. **132**, 182501 (2024).
[24] R. Elwell, C. Schneider, J. Jeet, J. E. S. Terhune, H. W. T. Morgan, A. N. Alexandrova, H. B. TranTan, A. Derevianko, and E. R. Hudson, Laser excitation of the $^{229}$Th nuclear isomeric transition in a solid-state host, Phys. Rev. Lett. **133**, 013201 (2024).
[25] C. Zhang *et al.*, Frequency ratio of the $^{229m}$Th nuclear isomeric transition and the $^{87}$Sr atomic clock, Nature (London) **633**, 63 (2024).
[26] S. Kraemer *et al.*, Observation of the radiative decay of the $^{229}$Th nuclear clock isomer, Nature (London) **617**, 706 (2023).
[27] R. Schwengner *et al.*, Photoexcitation of $^{76}$Ge, Phys. Rev. C **105**, 024303 (2022).
[28] U. Kneissl, H. H. Pitz, and A. Zilges, Investigation of nuclear structure by resonance fluorescence scattering, Prog. Part. Nucl. Phys. **37**, 349 (1996).
[29] A. Büchner *et al.*, The ELBE-project at Dresden-Rossendorf, in *Proceedings of EPAC 2000* (JACoW, Vienna, 2000).
[30] A. Makinaga *et al.*, Dipole strength of $^{181}$Ta for the evaluation of the $^{180}$Ta stellar neutron capture rate, Phys. Rev. C **90**, 044301 (2014).
[31] R. Massarczyk, G. Rusev, R. Schwengner, F. Donau, C. Bhatia, M. E. Gooden, J. H. Kelley, A. P. Tonchev, and W. Tornow, Magnetic dipole strength in $^{128}$Xe and $^{134}$Xe in the spin-flip resonance region, Phys. Rev. C **90**, 054310 (2014).
[32] A. Makinaga *et al.*, Dipole strength in $^{80}$Se for *s* process and nuclear transmutation of $^{79}$Se, Phys. Rev. C **94**, 044304 (2016).
[33] T. Shizuma *et al.*, Dipole strength distribution in $^{206}$Pb for the evaluation of the neutron-capture cross section of $^{205}$Pb, Phys. Rev. C **98**, 064317 (2018).

[34] R. Schwengner *et al.*, Electric and magnetic dipole strength in $^{66}$Zn, Phys. Rev. C **103**, 024312 (2021).

[35] X. Li, M. W. Ahmed, A. Banu, C. Bartram, B. Crowe, E. J. Downie, M. Emamian, G. Feldman, H. Gao *et al.*, Compton scattering from $^{4}$He at the TUNL HI$\gamma$S facility, Phys. Rev. C **101**, 034618 (2020).

[36] R. C. Runkle, A. E. Champagne, C. Angulo, C. Fox, C. Iliadis, R. Longland, and J. Pollanen, Direct measurement of the $^{14}$N$(p,\gamma)^{15}$O $S$ factor, Phys. Rev. Lett. **94**, 082503 (2005).

[37] S. Gales *et al.*, The extreme light infrastructure—nuclear physics (ELI-NP) facility: New horizons in physics with 10 PW ultra-intense lasers and 20 MeV brilliant gamma beams, Rep. Prog. Phys. **81**, 094301 (2018).

[38] V. Iancu *et al.*, Brilliant gamma beams for industrial applications: New opportunities, new challenges, J. Phys.: Conf. Ser. **763**, 012003 (2016).

[39] M. Bobeica *et al.*, Radioisotope production for medical applications at ELI-NP, Rom. Rep. Phys. **68**, S847 (2016).

[40] D. Budker *et al.*, Expanding nuclear physics horizons with the gamma factory, Ann. Phys. **534**, 2100284 (2022).

[41] D. Budker *et al.*, Atomic physics studies at the gamma factory at CERN, Ann. Phys. **532**, 2000204 (2020).

[42] V. Potapkin *et al.*, The $^{57}$Fe synchrotron Mössbauer source at the ESRF, J. Synchrotron Radiat. **19**, 559 (2012).

[43] T. Mitsui *et al.*, Development of an energy-domain $^{57}$Fe-Mössbauer spectrometer using synchrotron radiation and its application to ultrahigh-pressure studies with a diamond anvil cell, J. Synchrotron Radiat. **16**, 723 (2009).

[44] H.-C. Wille *et al.*, Nuclear resonant scattering at PETRA III: Brillant opportunities for nano – and extreme condition science, J. Phys.: Conf. Ser. **217**, 012008 (2010).

[45] P. Gütlich *et al.*, Mössbauer spectroscopy—an indispensable tool in solid state research, Spectroscopy Europe/World **24**, 21 (2012).

[46] W. Sturhahn, K. W. Quast, T. S. Toellner, E. E. Alp, J. Metge, and E. Gerdau, Electron emission from $^{57}$Fe nuclei excited with synchrotron radiation, Phys. Rev. B **53**, 171 (1996).

[47] T. Kawauchi *et al.*, Observation of internal-conversion electrons induced by inelastic nuclear resonant scattering, Appl. Surf. Sci. **256**, 962 (2009).

[48] M. Seto *et al.*, Observation of nuclear resonant scattering accompanied by phonon excitation using synchrotron radiation, Phys. Rev. Lett. **74**, 3828 (1995).

[49] R. Röhlsberger, *Nuclear Condensed Matter Physics with Synchrotron Radiation: Basic Principles, Methodology and Applications* (Springer, New York, 2004), Vol. 208.

[50] T. Masuda *et al.*, X-ray pumping of the $^{229}$Th nuclear clock isomer, Nature (London) **573**, 238 (2019).

[51] P. Emma *et al.*, First lasing and operation of an ångstrom-wavelength free-electron laser, Nat. Photon. **4**, 641 (2010).

[52] A. M. Kondratenko and E. L. Saldin, Generation of coherent radiation by a relativistic electron beam in an undulator, Particle Accelerators **10**, 207 (1980).

[53] C. Pellegrini, A 4 to 0.1 nm FEL based on the SLAC linac, *Proceedings of the Workshop on Fourth Generation Light Sources*, SSRL/SLAC Report, Vol. 92, No. 02 (1992), pp. 364–375.

[54] T. Ishikawa *et al.*, A compact x-ray free-electron laser emitting in the sub-ångström region, Nat. Photon. **6**, 540 (2012).

[55] C. Pellegrini, A. Marinelli, and S. Reiche, The physics of x-ray free-electron lasers, Rev. Mod. Phys. **88**, 015006 (2016).

[56] K. P. Heeg *et al.*, Spectral narrowing of x-ray pulses for precision spectroscopy with nuclear resonances, Science **357**, 375 (2017).

[57] Y. Shvyd'ko *et al.*, Resonant x-ray excitation of the nuclear clock isomer $^{45}$Sc, Nature (London) **622**, 471 (2023).

[58] L. von der Wense *et al.*, Direct detection of the $^{229}$Th nuclear clock transition, Nature (London) **533**, 47 (2016).

[59] P. G. Thirolf, B. Seiferle, and L. von der Wense, Improving our knowledge on the $^{229m}$Thorium isomer: Toward a test bench for time variations of fundamental constants, Ann. Phys. **531**, 1800381 (2019).

[60] R. W. Boyd, *Nonlinear Optics*, 4th ed. (Academic, New York, 2020).

[61] C. Li, *Nonlinear Optics* (Springer, Berlin, 2017).

[62] F. Belli *et al.*, Highly efficient deep UV generation by four-wave mixing in gas-filled hollow-core photonic crystal fiber, Opt. Lett. **44**, 5509 (2019).

[63] T. Togashi *et al.*, Generation of vacuum-ultraviolet light by an optically contacted, prism-coupled $KBe_2BO_3F_2$ crystal, Opt. Lett. **28**, 254 (2003).

[64] C. T. Chen, G. L. Wang, X. Y. Wang, and Z. Y. Xu, Deep-UV nonlinear optical crystal $KBe_2BO_3F_2$-discovery, growth, optical properties and applications, Appl. Phys. B **97**, 9 (2009).

[65] R. Hilbig and R. Wallenstein, Tunable VUV radiation generated by two-photon resonant frequency mixing in xenon, IEEE J. Quantum Electron. **19**, 194 (1983).

[66] A. Tünnermann *et al.*, Generation of tunable short pulse VUV radiation by four-wave mixing in xenon with femtosecond KrF-excimer laser pulses, IEEE J. Quantum Electron. **29**, 1233 (1993).

[67] S. J. Hanna *et al.*, A new broadly tunable (7.4–10.2 eV) laser based VUV light source and its first application to aerosol mass spectrometry, Int. J. Mass Spectrom. **279**, 134 (2009).

[68] J. Thielking *et al.*, Vacuum-ultraviolet laser source for spectroscopy of trapped thorium ions, New J. Phys. **25**, 083026 (2023).

[69] B. Seiferle *et al.*, Energy of the $^{229}$Th nuclear clock transition, Nature (London) **573**, 243 (2019).

[70] T. Sikorsky *et al.*, Measurement of the $^{229}$Th isomer energy with a magnetic microcalorimeter, Phys. Rev. Lett. **125**, 142503 (2020).

[71] G. C. Bjorklund, Effects of focusing on third-order nonlinear processes in isotropic media, IEEE J. Quantum Electron. **11**, 287 (1975).

[72] M. H. Hutchinson and K. J. Thomas, High-efficiency generation of narrow bandwidth tunable VUV radiation, IEEE J. Quantum Electron. **19**, 1823 (1983).

[73] R. Forbes *et al.*, Efficient (∼10%) generation of vacuum ultraviolet femtosecond pulses via four-wave mixing in hollow-core fibers, Opt. Lett. **49**, 3178 (2024).

[74] P. B. Corkum, Plasma perspective on strong field multiphoton ionization, Phys. Rev. Lett. **71**, 1994 (1993).

[75] K. J. Schafer, B. Yang, L. F. DiMauro, and K. C. Kulander, Above threshold ionization beyond the high harmonic cutoff, Phys. Rev. Lett. **70**, 1599 (1993).

[76] M. Nisoli *et al.*, Attosecond electron dynamics in molecules, Chem. Rev. **117**, 10760 (2017).

[77] A. Cingöz *et al.*, Direct frequency comb spectroscopy in the extreme ultraviolet, Nature (London) **482**, 68 (2012).

[78] C. Zhang *et al.*, Tunable VUV frequency comb for $^{229m}$Th nuclear spectroscopy, Opt. Lett. **47**, 5591 (2022).

[79] S. A. Diddams *et al.*, Optical frequency combs: Coherently uniting the electromagnetic spectrum, Science **369**, eaay3676 (2020).

[80] A. Baltuška, T. Fuji, and T. Kobayashi, Controlling the carrier-envelope phase of ultrashort light pulses with optical parametric amplifiers, Phys. Rev. Lett. **88**, 133901 (2002).

[81] Y. Lee *et al.*, Novel method for carrier-envelope-phase stabilization of femtosecond laser pulses, Opt. Express **13**, 2969 (2005).

[82] J.-F. Hergott *et al.*, Carrier-envelope phase stabilization of a 20 W, grating based, chirped-pulse amplified laser, using electro-optic effect in a $LiNbO_3$ crystal, Opt. Express **19**, 19935 (2011).

[83] H. R. Telle *et al.*, Carrier-envelope offset phase control: A novel concept for absolute optical frequency measurement and ultrashort pulse generation, Appl. Phys. B **69**, 327 (1999).

[84] T. Consortium, The thorium nuclear clock project (2020).

[85] P. G. Thirolf, S. Kraemer, D. Moritz, and K. Scharl, The thorium isomer $^{229m}$Th: Review of status and perspectives after more than 50 years of research, Eur. Phys. J. Spec. Top. **233**, 1113 (2024).

[86] M. Nisoli, S. D. Silvestri, and O. Svelto, Generation of high energy 10 fs pulses by a new pulse compression technique, Appl. Phys. Lett. **68**, 2793 (1996).

[87] J. M. Dudley, G. Genty, and S. Coen, Supercontinuum generation in photonic crystal fiber, Rev. Mod. Phys. **78**, 1135 (2006).

[88] R. Sollapur *et al.*, Resonance-enhanced multi-octave supercontinuum generation in antiresonant hollow-core fibers, Light: Sci. Applicat. **6**, e17124 (2017).

[89] J. C. Travers, T. Grigorova, C. Brahms, and F. Belli, High-energy pulse self-compression and ultraviolet generation through soliton dynamics in hollow capillary fibres, Nat. Photon. **13**, 547 (2019).

[90] C. Brahms, F. Belli, and J. C. Travers, Resonant dispersive wave emission in hollow capillary fibers filled with pressure gradients, Opt. Lett. **45**, 4456 (2020).

[91] T. Grigorova, C. Brahms, F. F. Belli, and J. C. Travers, Dispersion tuning of nonlinear optical pulse dynamics in gas-filled hollow capillary fibers, Phys. Rev. A **107**, 063512 (2023).

[92] L. Allen, M. W. Beijersbergen, R. J. C. Spreeuw, and J. P. Woerdman, Orbital angular momentum of light and the transformation of Laguerre-Gaussian laser modes, Phys. Rev. A **45**, 8185 (1992).

[93] S. Franke-Arnold, Optical angular momentum and atoms, Philos. Trans. R. Soc. A **375**, 20150435 (2017).

[94] K. Y. Bliokh, F. J. Rodriguez-Fortuno, F. Nori, and A. V. Zayats, Spin–orbit interactions of light, Nat. Photon. **9**, 796 (2015).

[95] H. M. Scholz-Marggraf, S. Fritzsche, V. G. Serbo, A. Afanasev, and A. Surzhykov, Absorption of twisted light by hydrogenlike atoms, Phys. Rev. A **90**, 013425 (2014).

[96] A. Surzhykov, D. Seipt, V. G. Serbo, and S. Fritzsche, Interaction of twisted light with many-electron atoms and ions, Phys. Rev. A **91**, 013403 (2015).

[97] S. A.-L. Schulz, A. A. Peshkov, R. A. Muller, R. Lange, N. Huntemann, C. Tamm, E. Peik, and A. Surzhykov, Generalized excitation of atomic multipole transitions by twisted light modes, Phys. Rev. A **102**, 012812 (2020).

[98] T. Kirschbaum, T. Schumm, and A. Pálffy, Photoexcitation of the $^{229}$Th nuclear clock transition using twisted light, Phys. Rev. C **110**, 064326 (2024).

[99] M. Solyanik-Gorgone *et al.*, Excitation of E1-forbidden atomic transitions with electric, magnetic, or mixed multipolarity in light fields carrying orbital and spin angular momentum [invited], J. Opt. Soc. Am. B **36**, 565 (2019).

[100] L. von der Wense and B. Seiferle, The $^{229}$Th isomer: Prospects for a nuclear optical clock, Eur. Phys. J. A **56**, 277 (2020).

[101] S. J. Herr *et al.*, Fanout periodic poling of $BaMgF_4$ crystals, Opt. Mater. Express **13**, 2158 (2023).

[102] V. S. Malinovsky and J. L. Krause, General theory of population transfer by adiabatic rapid passage with intense, chirped laser pulses, Eur. Phys. J. D **14**, 147 (2001).

[103] T. Kirschbaum, N. Minkov, and A. Pálffy, Nuclear coherent population transfer to the $^{229}$Th isomer using x-ray pulses, Phys. Rev. C **105**, 064313 (2022).

[104] E. Kuznetsova, G. Liu, and S. A. Malinovskaya, Adiabatic rapid passage two-photon excitation of a Rydberg atom, Phys. Scr. **2014**, 014024 (2014).

[105] K. Li, D. C. Spierings, and A. M. Steinberg, Efficient adiabatic rapid passage in the presence of noise, Phys. Rev. A **108**, 012615 (2023).

[106] N. Chanda, P. Patnaik, and R. Bhattacharyya, Optimal population transfer using adiabatic rapid passage in the presence of drive-induced dissipation, Phys. Rev. A **107**, 063708 (2023).

[107] T. J. Bürvenich, J. Evers, and C. H. Keitel, Nuclear quantum optics with x-ray laser pulses, Phys. Rev. Lett. **96**, 142501 (2006).

[108] T. J. Bürvenich, J. Evers, and C. H. Keitel, Dynamic nuclear stark shift in superintense laser fields, Phys. Rev. C **74**, 044601 (2006).

[109] W.-T. Liao, A. Palffy, and C. H. Keitel, Nuclear coherent population transfer with x-ray laser pulses, Phys. Lett. B **705**, 134 (2011).

[110] K. Beeks *et al.*, Growth and characterization of thorium-doped calcium fluoride single crystals, Sci. Rep. **13**, 3897 (2023).

[111] R. Röhlsberger, H.-C. Wille, K. Schlage, and B. Sahoo, Electromagnetically induced transparency with resonant nuclei in a cavity, Nature (London) **482**, 199 (2012).

[112] M. E. Rose, Internal conversion theory, in *Internal Conversion Processes*, edited by J. H. Hamilton (Academic Press, New York, 1966), Chap. II, pp. 15–33.

[113] T. Kibédi *et al.*, Evaluation of theoretical conversion coefficients using BrIcC, Phys. Res. A **589**, 202 (2008).

[114] C. J. Campbell, A. G. Radnaev, A. Kuzmich, V. A. Dzuba, V. V. Flambaum, and A. Derevianko, Single-ion nuclear clock for metrology at the 19th decimal place, Phys. Rev. Lett. **108**, 120802 (2012).

[115] E. Peik and C. Tamm, Nuclear laser spectroscopy of the 3.5 eV transition in Th-229, Europhys. Lett. **61**, 181 (2003).

[116] E. V. Tkalya, Proposal for a nuclear gamma-ray laser of optical range, Phys. Rev. Lett. **106**, 162501 (2011).

[117] W.-T. Liao, S. Das, C. H. Keitel, and A. Palffy, Coherence-enhanced optical determination of the $^{229}$Th isomeric transition, Phys. Rev. Lett. **109**, 262502 (2012).

[118] P. Borisyuk *et al.*, Band structure and decay channels of thorium-229 low-lying isomeric state for ensemble of thorium

atoms adsorbed on calcium fluoride, Phys. Status Solidi C **12**, 1333 (2015).
[119] E. V. Tkalya, A. N. Zherikhin, and V. I. Zhudov, Decay of the low-energy nuclear isomer $^{229}$Th$^{m}$ ($3/2^{+}$, $3.5 \pm 1.0$ eV) in solids, dielectrics and metals: A new scheme of experimental research, Phys. Rev. C **61**, 064308 (2000).
[120] F. F. Karpeshin and M. B. Trzhaskovskaya, Impact of the electron environment on the lifetime of the $^{229}$Th$^{m}$ low-lying isomer, Phys. Rev. C **76**, 054313 (2007).
[121] V. F. Strizhov and E. V. Tkalya, Decay channel of low-lying isomer state of the $^{229}$Th nucleus. Possibilities of experimental investigation, Sov. Phys. JETP **72**, 387 (1991).
[122] P. V. Bilous, G. A. Kazakov, I. D. Moore, T. Schumm, and A. Palffy, Internal conversion from excited electronic states of $^{229}$Th ions, Phys. Rev. A **95**, 032503 (2017).
[123] F. F. Karpeshin and M. B. Trzhaskovskaya, Bound internal conversion versus nuclear excitation by electron transition: Revision of the theory of optical pumping of the $^{229m}$Th isomer, Phys. Rev. C **95**, 034310 (2017).
[124] S. G. Johnson *et al.*, Resonance ionization mass spectrometry of thorium: Determination of the autoionization level structure and a re-determination of the ionization potential, Spectrochim. Acta Part B: Atomic Spectrosc. **47**, 633 (1992).
[125] S. Köhler *et al.*, Determination of the first ionization potential of actinide elements by resonance ion-ization mass spectroscopy, Spectrochim. Acta, Part B: Atom.c Spectrosc. **52**, 717 (1997).
[126] NIST, NIST atomic spectra database ionization energies form (2025), https://physics.nist.gov/PhysRefData/ASD/ionEnergy.html.
[127] B. Seiferle, L. von der Wense, and P. G. Thirolf, Lifetime measurement of the $^{229}$Th nuclear isomer, Phys. Rev. Lett. **118**, 042501 (2017).
[128] F. Karpeshin, Resonance internal conversion as a way of accelerating nuclear processes, Phys. Part. Nuclei **37**, 284 (2006).
[129] H. Zhang and X. Wang, Theory of isomeric excitation of $^{229}$Th via electronic processes, Front. Phys. **11**, 1166566 (2023).
[130] E. V. Tkalya, Probability of nonradiative excitation of nuclei in transitions of an electron in an atomic shell, Sov. Phys.–JETP **75**, 200 (1992).
[131] S. G. Porsev and V. V. Flambaum, Electronic bridge process in $^{229}$Th$^{+}$, Phys. Rev. A **81**, 042516 (2010).
[132] S. G. Porsev, V. V. Flambaum, E. Peik, and C. Tamm, Excitation of the isomeric $^{229m}$Th nuclear state via an electronic bridge process in $^{229}$Th$^{+}$, Phys. Rev. Lett. **105**, 182501 (2010).
[133] P. V. Bilous, E. Peik, and A. Pálffy, Laser-induced electronic bridge for characterization of the $^{229m}$Th $\rightarrow$ $^{229g}$Th nuclear transition with a tunable optical laser, New J. Phys. **20**, 013016 (2018).
[134] A. Y. Dzyublik, Excitation of $^{229m}$Th in the electron bridge via continuum, as a scattering process, Phys. Rev. C **102**, 024604 (2020).
[135] P. Bilous, H. Bekker, J. C. Berengut, B. Seiferle, L. von der Wense, P. G. Thirolf, T. Pfeifer, J. R. Crespo Lopez-Urrutia, and A. Palffy, Electronic bridge excitation in highly charged $^{229}$Th ions, Phys. Rev. Lett. **124**, 192502 (2020).
[136] B. S. Nickerson, M. Pimon, P. V. Bilous, J. Gugler, K. Beeks, T. Sikorsky, P. Mohn, T. Schumm, and A. Palffy, Nuclear excitation of the $^{229}$Th isomer via defect states in doped crystals, Phys. Rev. Lett. **125**, 032501 (2020).
[137] E. V. Tkalya, Excitation of $^{229m}$Th at inelastic scattering of low energy electrons, Phys. Rev. Lett. **124**, 242501 (2020).
[138] H. Zhang, W. Wang, and X. Wang, Nuclear excitation cross section of $^{229}$Th via inelastic electron scattering, Phys. Rev. C **106**, 044604 (2022).
[139] E. V. Tkalya, Cross section of the Coulomb excitation of $^{229}$Th by low energy muons, Chin. Phys. C **45**, 094102 (2021).
[140] W. Wang, J. Zhou, B. Liu, and X. Wang, Exciting the isomeric $^{229}$Th nuclear state via laser-driven electron recollision, Phys. Rev. Lett. **127**, 052501 (2021).
[141] W. Wang, H. Zhang, and X. Wang, Strong-field atomic physics meets $^{229}$Th nuclear physics, J. Phys. B: At. Mol. Opt. Phys. **54**, 244001 (2021).
[142] X. Wang, Nuclear excitation of $^{229}$Th induced by laser-driven electron recollision, Phys. Rev. C **106**, 024606 (2022).
[143] D. Lentrodt, C. H. Keitel, and J. Evers, Towards nonlinear optics with Mössbauer nuclei using x-ray cavities, Phys. Rev. Lett. **135**, 033801 (2025).
[144] G. C. Baldwin, J. C. Solem, and V. I. Gol'danskii, Approaches to the development of gamma-ray lasers, Rev. Mod. Phys. **53**, 687 (1981).
[145] R. L. Mössbauer, Recoilless nuclear resonance absorption of gamma radiation, Science **137**, 731 (1962).
[146] O. Kocharovskaya, Amplification and lasing without inversion, Phys. Rep. **219**, 175 (1992).
[147] G. C. Baldwin and J. C. Solem, Recoilless gamma-ray lasers, Rev. Mod. Phys. **69**, 1085 (1997).
[148] R. Röhlsberger *et al.*, Collective lamb shift in single-photon superradiance, Science **328**, 1248 (2010).
[149] K. P. Heeg *et al.*, Vacuum-assisted generation and control of atomic coherences at x-ray energies, Phys. Rev. Lett. **111**, 073601 (2013).
[150] K. P. Heeg *et al.*, Interferometric phase detection at x-ray energies via Fano resonance control, Phys. Rev. Lett. **114**, 207401 (2015).
[151] K. P. Heeg *et al.*, Tunable subluminal propagation of narrow-band x-ray pulses, Phys. Rev. Lett. **114**, 203601 (2015).
[152] J. Haber, K. Schulze, K. Schlage *et al.*, Collective strong coupling of x-rays and nuclei in a nuclear optical lattice, Nat. Photon. **10**, 445 (2016).
[153] J. Haber, X. Kong, C. Strohm *et al.*, Rabi oscillations of x-ray radiation between two nuclear ensembles, Nat. Photon. **11**, 720 (2017).
[154] F. Vagizov *et al.*, Coherent control of the waveforms of recoilless gamma-ray photons, Nature (London) **508**, 80 (2014).
[155] I. Georgescu, The first decade of XFELs, Nat. Rev. Phys. **2**, 345 (2020).
[156] I. Matsuda and R. Arafune, *Nonlinear X-ray Spectroscopy for Materials Science*, Springer Series in Optical Sciences, Vol. 246 (Springer, Berlin, 2023).
[157] N. Rohringer, X-ray raman scattering: A building block for nonlinear spectroscopy, Philos. Trans. R. Soc. A **377**, 20170471 (2019).
[158] S. Sofer *et al.*, Quantum enhanced x-ray detection, Phys. Rev. X **9**, 031033 (2019).
[159] S. Nandi *et al.*, Observation of Rabi dynamics with a short-wavelength free-electron laser, Nature (London) **608**, 488 (2022).
[160] G. Doumy *et al.*, Nonlinear atomic response to intense ultrashort x rays, Phys. Rev. Lett. **106**, 083002 (2011).

[161] N. Rohringer *et al.*, Atomic inner-shell x-ray laser at 1.46 nanometres pumped by an x-ray free-electron laser, Nature (London) **481**, 488 (2012).

[162] M. Kalvius and P. Kienle, *The Rudolf Mössbauer Story: His Scientific Work and its Impact on Science and History* (Springer, Berlin, 2012).

[163] Y. Yoshida and G. Langouche, *Modern Mössbauer Spectroscopy*, Topics in Applied Physics (Springer, Singapore, 2021).

[164] R. Röhlsberger and J. Evers, Quantum optical phenomena in nuclear resonant scattering, in *Modern Mössbauer Spectroscopy: New Challenges Based on Cutting-Edge Techniques*, edited by Y. Yoshida and G. Langouche (Springer, Singapore, 2021), pp. 105–171.

[165] L. Wolff and J. Evers, Characterization and detection method for x-ray excitation of Mössbauer nuclei beyond the low-excitation regime, Phys. Rev. A **108**, 043714 (2023).

[166] M. Fleischhauer, A. Imamoglu, and J. P. Marangos, Electromagnetically induced transparency: Optics in coherent media, Rev. Mod. Phys. **77**, 633 (2005).

[167] C. Buth, R. Santra, and L. Young, Electromagnetically induced transparency for x-rays, Phys. Rev. Lett. **98**, 253001 (2007).

[168] T. Glover *et al.*, Controlling x-rays with light, Nat. Phys. **6**, 69 (2010).

[169] R. E. Holland, F. J. Lynch, and K. E. Nystén, Lifetimes of d3/2 hole states in scandium isotopes, Phys. Rev. Lett. **13**, 241 (1964).

[170] S. Liu *et al.*, Cascaded hard x-ray self-seeded free-electron laser at megahertz repetition rate, Nat. Photon. **17**, 984 (2023).

[171] V. Goldanskii and V. Namiot, On the excitation of isomeric nuclear levels by laser radiation through inverse internal electron conversion, Phys. Lett. B **62**, 393 (1976).

[172] A. Pálffy, Nuclear effects in atomic transitions, Contemp. Phys. **51**, 471 (2010).

[173] N. Cue, J.-C. Poizat, and J. Remillieux, Exciting the nucleus by target electron capture into atomic orbitals, Europhys. Lett. **8**, 19 (1989).

[174] P. Walker and G. Dracoulis, Energy traps in atomic nuclei, Nature (London) **399**, 35 (1999).

[175] P. Walker and J. Carroll, Ups and downs of nuclear isomers, Phys. Today **58**(6), 39 (2005).

[176] A. Zadernovsky and J. Carroll, Non-radiative triggering of long-lived nuclear isomers, Hyperfine Interact. **143**, 153 (2002).

[177] J. Carroll and C. Chiara, Isomer depletion, Eur. Phys. J. Spec. Top. **233**, 1151 (2024).

[178] J. Zhao, A. Pálffy, C. H. Keitel, and Y. Wu, Efficient production of $^{229m}$Th via nuclear excitation by electron capture, Phys. Rev. C **110**, 014330 (2024).

[179] J. Qi, H. Zhang, and X. Wang, Isomeric excitation of $^{229}$Th in laser-heated clusters, Phys. Rev. Lett. **130**, 112501 (2023).

[180] K. Słabkowska, L. Syrocki, M. Polasik, J. J. Carroll, C. J. Chiara, and J. Rzadkiewicz, Dominant magnetic-dipole nuclear excitation by electron capture in a beam-based scenario for the $^{84m}$Rb isomer, Phys. Rev. C **109**, 054327 (2024).

[181] C. Chiara *et al.*, Isomer depletion as experimental evidence of nuclear excitation by electron capture, Nature (London) **554**, 216 (2018).

[182] Y. Wu, C. H. Keitel, and A. Pálffy, $^{93m}$Mo isomer depletion via beam-based nuclear excitation by electron capture, Phys. Rev. Lett. **122**, 212501 (2019).

[183] J. Rzadkiewicz, M. Polasik, K. Slabkowska, L. Syrocki, J. J. Carroll, and C. J. Chiara, Novel approach to $^{93m}$Mo isomer depletion, Phys. Rev. Lett. **127**, 042501 (2021).

[184] J. Rzadkiewicz *et al.*, $^{93m}$Mo isomer depletion via nuclear excitation by electron capture in resonant transfer into highly excited open-shell atomic states, Phys. Rev. C **108**, L031302 (2023).

[185] X. Z. S. Guo, Y. Fang, and C. Petrache, Possible overestimation of isomer depletion due to contamination, Nature (London) **594**, E1 (2021).

[186] C. Chiara *et al.*, Reply to: Possible overestimation of isomer depletion due to contamination, Nature (London) **594**, E3 (2021).

[187] S. Guo *et al.*, Probing $^{93m}$Mo isomer depletion with an isomer beam, Phys. Rev. Lett. **128**, 242502 (2022).

[188] M. Morita, Nuclear excitation by electron transition and its application to uranium 235 separation, Prog. Theor. Phys. **49**, 1574 (1973).

[189] S. Kishimoto, Y. Yoda, M. Seto, Y. Kobayashi, S. Kitao, R. Haruki, T. Kawauchi, K. Fukutani, and T. Okano, Observation of nuclear excitation by electron transition in $^{197}$Au with synchrotron x rays and an avalanche photodiode, Phys. Rev. Lett. **85**, 1831 (2000).

[190] I. Ahmad, R. W. Dunford, H. Esbensen, D. S. Gemmell, E. P. Kanter, U. Rutt, and S. H. Southworth, Nuclear excitation by electronic transition in $^{189}$Os, Phys. Rev. C **61**, 051304(R) (2000).

[191] T. Saito *et al.*, Nuclear excitation by electron transition (NEET) in $^{237}$Np following k-shell photoionization, Phys. Lett. B **92**, 293 (1980).

[192] M. Harston, Analysis of probabilities for nuclear excitation by near-resonant electronic transitions, Nucl. Phys. A **690**, 447 (2001).

[193] E. V. Tkalya, Factors responsible for the difference of the theoretical and experimental probability for nuclear excitation by electron transition, JETP Lett. **56**, 131 (1992).

[194] E. V. Tkalya, Dynamical effect of finite nuclear size in the nuclear excitation process during electron transitions in an atomic shell, JETP **78**, 239 (1994).

[195] G. Claverie *et al.*, Search for nuclear excitation by electronic transition in $^{235}$U, Phys. Rev. C **70**, 044303 (2004).

[196] P. A. Chodash, J. T. Harke, E. B. Norman, S. C. Wilks, R. J. Casperson, S. E. Fisher, K. S. Holliday, J. R. Jeffries, and M. A. Wakeling, Nuclear excitation by electronic transition of $^{235}$U, Phys. Rev. C **93**, 034610 (2016).

[197] F. Karpeshin, I. Band, M. Trzhaskovskaya, and M. Listengarten, Optical pumping $^{229m}$Th through NEET as a new effective way of producing nuclear isomers, Phys. Lett. B **372**, 1 (1996).

[198] V. Krutov and V. Fomenko, Influence of electronic shell on gamma radiation of atomic nuclei, Ann. Phys. **476**, 291 (1968).

[199] V. Krutov, On the theory of internal conversion. I, Bull. Acad. Sci. USSR (Phys. Ser.) **22**, 159 (1958).

[200] V. Krutov and K. Müller, On the internal conversion theory. II. Bull. Acad. Sci. USSR (Phys. Ser.) **22**, 168 (1958).

[201] D. Kekez, A. Ljubici, K. Pisk, and B. A. Logan, Nuclear deexcitation via the electronic-bridge mechanism, Phys. Rev. Lett. **55**, 1366 (1985).
[202] D. Kekez, K. Pisk, A. Ljubicic, and B. A. Logan, Nuclear deexcitation via an inelastic electronic bridge, Phys. Rev. C **34**, 1446 (1986).
[203] F. F. Karpeshin, I. M. Band, M. B. Trzhaskovskaya, and B. A. Zon, Study of $^{229}$Th through laser-induced resonance internal conversion, Phys. Lett. B **282**, 267 (1992).
[204] S. G. Porsev and V. V. Flambaum, Effect of atomic electrons on the 7.6-eV nuclear transition in $^{229}Th^{3+}$, Phys. Rev. A **81**, 032504 (2010).
[205] N. Q. Cai, G. Q. Zhang, C. B. Fu *et al.*, Populating $^{229m}$Th via two-photon electronic bridge mechanism, Nucl. Sci. Tech. **32**, 59 (2021).
[206] L. Li, Z. Li, C. Wang *et al.*, Scheme for the excitation of thorium-229 nuclei based on electronic bridge excitation, Nucl. Sci. Tech. **34**, 24 (2023).
[207] R. A. Müller, A. V. Volotka, S. Fritzsche, and A. Surzhykov, Theoretical analysis of the electron bridge process in $^{229}Th^{3+}$, Nucl. Instrum. Methods Phys. Res. Sect. B **408**, 84 (2017).
[208] C. J. Campbell, A. G. Radnaev, and A. Kuzmich, Wigner crystals of $^{229}$Th for optical excitation of the nuclear isomer, Phys. Rev. Lett. **106**, 223001 (2011).
[209] L. Eisenbud, The formal properties of nuclear collisions, Ph.D. thesis, Princeton University, 1948.
[210] E. P. Wigner, Lower limit for the energy derivative of the scattering phase shift, Phys. Rev. **98**, 145 (1955).
[211] F. T. Smith, Lifetime matrix in collision theory, Phys. Rev. **119**, 2098 (1960).
[212] P.-M. Paul *et al.*, Observation of a train of attosecond pulses from high harmonic generation, Science **292**, 1689 (2001).
[213] J. Itatani, F. Quere, G. L. Yudin, M. Y. Ivanov, F. Krausz, and P. B. Corkum, Attosecond streak camera, Phys. Rev. Lett. **88**, 173903 (2002).
[214] M. Drescher *et al.*, X-ray pulses approaching the attosecond frontier, Science **291**, 1923 (2001).
[215] R. Pazourek, S. Nagele, and J. Burgdörfer, Attosecond chronoscopy of photoemission, Rev. Mod. Phys. **87**, 765 (2015).
[216] R. Trebino *et al.*, Measuring ultrashort laser pulses in the time-frequency domain using frequency-resolved optical gating, Rev. Sci. Instrum. **68**, 3277 (1997).
[217] Y. Mairesse and F. Quéré, Frequency-resolved optical gating for complete reconstruction of attosecond bursts, Phys. Rev. A **71**, 011401(R) (2005).
[218] Y. Mairesse *et al.*, Attosecond synchronization of high-harmonic soft x-rays, Science **302**, 1540 (2003).
[219] S. Kazamias and P. Balcou, Intrinsic chirp of attosecond pulses: Single-atom model versus experiment, Phys. Rev. A **69**, 063416 (2004).
[220] S. Nagele *et al.*, Time-resolved photoemission by attosecond streaking: Extraction of time information, J. Phys. B: At. Mol. Opt. Phys. **44**, 081001 (2011).
[221] J. Fuchs *et al.*, Time delays from one-photon transitions in the continuum, Optica **7**, 154 (2020).
[222] M. Schultze *et al.*, Delay in photoemission, Science **328**, 1658 (2010).
[223] K. Klünder, J. M. Dahlstrom, M. Gisselbrecht, T. Fordell, M. Swoboda, D. Guenot, P. Johnsson, J. Caillat, J. Mauritsson, A. Maquet, R. Taieb, and A. LHuillier, Probing single-photon ionization on the attosecond time scale, Phys. Rev. Lett. **106**, 143002 (2011).
[224] J. M. Dahlström, A. L'Huillier, and A. Maquet, Introduction to attosecond delays in photoionization, J. Phys. B: At. Mol. Opt. Phys. **45**, 183001 (2012).
[225] M. Isinger *et al.*, Photoionization in the time and frequency domain, Science **358**, 893 (2017).
[226] L. Cattaneo *et al.*, Comparison of attosecond streaking and RABBITT, Opt. Express **24**, 29060 (2016).
[227] M. Huppert, I. Jordan, D. Baykusheva, A. von Conta, and H. J. Worner, Attosecond delays in molecular photoionization, Phys. Rev. Lett. **117**, 093001 (2016).
[228] A. Chacon, M. Lein, and C. Ruiz, Asymmetry of Wigner's time delay in a small molecule, Phys. Rev. A **89**, 053427 (2014).
[229] J. Vos *et al.*, Orientation-dependent stereo Wigner time delay and electron localization in a small molecule, Science **360**, 1326 (2018).
[230] S. Biswas *et al.*, Probing molecular environment through photoemission delays, Nat. Phys. **16**, 778 (2020).
[231] S. Beaulieu *et al.*, Attosecond-resolved photoionization of chiral molecules, Science **358**, 1288 (2017).
[232] H. Ahmadi *et al.*, Attosecond photoionisation time delays reveal the anisotropy of the molecular potential in the recoil frame, Nat. Commun. **13**, 1242 (2022).
[233] A. J. Suñer-Rubio *et al.*, Attosecond photoionization delays in molecules: The role of nuclear motion, Phys. Rev. Res. **6**, L022066 (2024).
[234] V. Loriot *et al.*, Attosecond metrology of the two-dimensional charge distribution in molecules, Nat. Phys. **20**, 765 (2024).
[235] I. Jordan *et al.*, Attosecond spectroscopy of liquid water, Science **369**, 974 (2020).
[236] A. L. Cavalieri *et al.*, Attosecond spectroscopy in condensed matter, Nature (London) **449**, 1029 (2007).
[237] R. Locher *et al.*, Energy-dependent photoemission delays from noble metal surfaces by attosecond interferometry, Optica **2**, 405 (2015).
[238] M. Ossiander *et al.*, Absolute timing of the photoelectric effect, Nature (London) **561**, 374 (2018).
[239] M. Lucchini *et al.*, Light-matter interaction at surfaces in the spatiotemporal limit of macroscopic models, Phys. Rev. Lett. **115**, 137401 (2015).
[240] U. Fano, Sullo spettro di assorbimento dei gas nobili presso il limite dello spettro d'arco, Nuovo Cimento **12**, 154 (1935).
[241] U. Fano, Effects of configuration interaction on intensities and phase shifts, Phys. Rev. **124**, 1866 (1961).
[242] M. Kotur *et al.*, Spectral phase measurement of a Fano resonance using tunable attosecond pulses, Nat. Commun. **7**, 10566 (2016).
[243] C. Cirelli *et al.*, Anisotropic photoemission time delays close to a Fano resonance, Nat. Commun. **9**, 955 (2018).
[244] M. Wickenhauser, J. Burgdörfer, F. Krausz, and M. Drescher, Time resolved Fano resonances, Phys. Rev. Lett. **94**, 023002 (2005).
[245] R. Borrego-Varillas and M. Lucchini, Reconstruction of atomic resonances with attosecond streaking, Opt. Express **29**, 9711 (2021).

[246] V. Gruson *et al.*, Attosecond dynamics through a Fano resonance: Monitoring the birth of a photoelectron, Science **354**, 734 (2016).
[247] H. W. Kroto *et al.*, $C_{60}$: Buckminsterfullerene, Nature (London) **318**, 162 (1985).
[248] I. V. Hertel, H. Steger, J. de Vries, B. Weisser, C. Menzel, B. Kamke, and W. Kamke, Giant plasmon excitation in free $C_{60}$ and $C_{70}$ molecules studied by photoionization, Phys. Rev. Lett. **68**, 784 (1992).
[249] S. Biswas *et al.*, Correlation-driven attosecond photoemission delay in the plasmonic excitation of $C_{60}$ fullerene, Sci. Adv. **11**, eads0494 (2025).
[250] M. Drescher *et al.*, Time-resolved atomic inner-shell spectroscopy, Nature (London) **419**, 803 (2002).
[251] M. Ossiander *et al.*, Attosecond correlation dynamics, Nat. Phys. **13**, 280 (2017).
[252] S. Li *et al.*, Attosecond coherent electron motion in Auger-Meitner decay, Science **375**, 285 (2022).
[253] L. S. Cederbaum *et al.*, Ultrafast charge migration by electron correlation, Chem. Phys. Lett. **307**, 205 (1999).
[254] V. Despré, N. V. Golubev, and A. I. Kuleff, Charge migration in propiolic acid: A full quantum dynamical study, Phys. Rev. Lett. **121**, 203002 (2018).
[255] M. Vacher, L. Steinberg, A. J. Jenkins, M. J. Bearpark, and M. A. Robb, Electron dynamics following photoionization: Decoherence due to the nuclear-wave-packet width, Phys. Rev. A **92**, 040502(R) (2015).
[256] M. Vacher *et al.*, Communication: Oscillating charge migration between lone pairs persists without significant interaction with nuclear motion in the glycine and Gly-Gly-NH-$CH_3$ radical cations, J. Chem. Phys. **140**, 201102 (2014).
[257] M. Lara-Astiaso *et al.*, Decoherence, control and attosecond probing of XUV-induced charge migration in biomolecules. A theoretical outlook, Faraday Discuss. **194**, 41 (2016).
[258] A. S. Folorunso *et al.*, Attochemistry regulation of charge migration, J. Phys. Chem. A **127**, 1894 (2023).
[259] J. Breidbach and L. S. Cederbaum, Universal attosecond response to the removal of an electron, Phys. Rev. Lett. **94**, 033901 (2005).
[260] F. Remacle and R. D. Levine, An electronic time scale in chemistry, Proc. Natl. Acad. Sci. USA **103**, 6793 (2006).
[261] A. I. Kuleff and L. S. Cederbaum, Ultrafast correlation-driven electron dynamics, J. Phys. B: At. Mol. Opt. Phys. **47**, 124002 (2014).
[262] F. Calegari *et al.*, Ultrafast electron dynamics in phenylalanine initiated by attosecond pulses, Science **346**, 336 (2014).
[263] M. Lara-Astiaso *et al.*, Attosecond pump–probe spectroscopy of charge dynamics in tryptophan, J. Phys. Chem. Lett. **9**, 4570 (2018).
[264] E. P. Månsson *et al.*, Real-time observation of a correlation-driven sub 3 fs charge migration in ionised adenine, Commun. Chem. **4**, 73 (2021).
[265] E. P. Månsson *et al.*, Ultrafast dynamics of adenine following XUV ionization, J. Phys. Photonics **4**, 034003 (2022).
[266] D. Schwickert *et al.*, Charge-induced chemical dynamics in glycine probed with time-resolved auger electron spectroscopy, Struct. Dyn **9**, 064301 (2022).
[267] P. M. Kraus *et al.*, Measurement and laser control of attosecond charge migration in ionized iodoacetylene, Science **350** 790 (2015).
[268] D. T. Matselyukh *et al.*, Decoherence and revival in attosecond charge migration driven by non-adiabatic dynamics, Nat. Phys. **18**, 1206 (2022).
[269] V. Wanie *et al.*, Capturing electron-driven chiral dynamics in UV-excited molecules, Nature (London) **630**, 109 (2024).
[270] O. Kühn and V. May, *Charge and Energy Transfer Dynamics in Molecular Systems* (WileyHoboken, NJ, 2023).
[271] J. Gunst, Y. A. Litvinov, C. H. Keitel, and A. Pálffy, Dominant secondary nuclear photoexcitation with the x-ray free-electron laser, Phys. Rev. Lett. **112**, 082501 (2014).
[272] Y. Wu, J. Gunst, C. H. Keitel, and A. Pálffy, Tailoring laser-generated plasmas for efficient nuclear excitation by electron capture, Phys. Rev. Lett. **120**, 052504 (2018).
[273] F. Salvat and J. Parellada, Theory of conversion electron Mössbauer spectroscopy (CEMS), Nucl. Instrum. Methods Phys. Res. Sect. B **1**, 70 (1984).
[274] A. Pálffy, W. Scheid, and Z. Harman, Theory of nuclear excitation by electron capture for heavy ions, Phys. Rev. A **73**, 012715 (2006).
[275] A. Pálffy, J. Evers, and C. H. Keitel, Isomer triggering via nuclear excitation by electron capture, Phys. Rev. Lett. **99**, 172502 (2007).
[276] J. Baró, J. Sempau, J. Fernández-Varea, and F. Salvat, PENELOPE: An algorithm for Monte Carlo simulation of the penetration and energy loss of electrons and positrons in matter, Nucl. Instrum. Methods Phys. Res. Sect. B **100**, 31 (1995).
[277] A. V. K. Nomura and Y. Ujihira, Applications of conversion electron Mössbauer spectrometry (CEMS), J. Radiol. Nucl. Chem. **202**, 103 (1996).
[278] Y. Wu, S. Gargiulo, F. Carbone, C. H. Keitel, and A. Pálffy, Dynamical control of nuclear isomer depletion via electron vortex beams, Phys. Rev. Lett. **128**, 162501 (2022).
[279] T. Spillane *et al.*, $^{12}C + {}^{12}C$ Fusion reactions near the Gamow energy, Phys. Rev. Lett. **98**, 122501 (2007).
[280] A. Pálffy *et al.*, Nuclear excitation by electron capture followed by fast x-ray emission, Phys. Lett. B **661**, 330 (2008).
[281] Z. Bonchev, A. Jordanov, and A. Minkova, Method of analysis of thin surface layers by the Mössbauer effect, Nucl. Instrum. Methods **70**, 36 (1969).
[282] K. R. Swanson and J. J. Spijkerman, Analysis of thin surface layers by Fe-57 Mössbauer backscattering spectrometry, J. Appl. Phys. **41**, 3155 (1970).
[283] J. R. Gancedo, M. Gracia, and J. F. Marco, Cems methodology, Hyperfine Interact. **66**, 83 (1991).
[284] J. J. Spijkerman, in *Mössbauer Effect Methodology*, edited by I. J. Gruvennan (Plenum, New York, 1971), p. 85.
[285] M. J. Tricker, in *Mössbauer Spectroscopy and its Chemical Spplications*, edited by J. G. Stevens and G. K. Shenoy (ACSWashington, DC, 1981).
[286] J. Sawicki and B. Sawicka, Experimental techniques for conversion electron Mössbauer spectroscopy, Hyperfine Interact. **13**, 199 (1983).
[287] W. Meisel, Phase analysis of surface layers by Mössbauer spectroscopy, Spectrochim. Acta Part B: Atom. Spectrosc. **39**, 1505 (1984).
[288] M. Inaba, K. Nomura, and Y. Ujihara, Sensitive area of a back-scatter-type gas flow detector for conversion electron Mössbauer spectrometry, J. Phys. Colloques **41**, C1-115 (1980).

[289] K. Nomura, M. Tasaka, and Y. Ujihira, Application of conversion electron Mössbauer spectrometry to corrosion studies, Corrosion **44**, 131 (1988).
[290] K. Nomura and Y. Ujihira, *Applications of the Mössbauer Effect* (Gordon and Breach, New York, 1985), pp. 1185–1192.
[291] K. Nomura and Y. Ujihira, Analysis of black layers on steel using conversion electron Mössbauer spectrometry, J. Mater. Sci. **19**, 2664 (1984).
[292] P. Refait, P. Bauer, and J. M. R. Genin, The transformation of green rust one into fe(II)-fe(III) hydroxides — fe(II)-fe(III) oxyhydroxides by oxidation, Hyperfine Interact. **69**, 831 (1992).
[293] J. Lipka *et al.*, Mössbauer study of amorphous and nanocrystalline fe-cu-nb-si-b alloys, Hyperfine Interact. **57**, 1969 (1990).
[294] N. R. Bulakh *et al.*, Mössbauer studies of fe-doped sno2 semiconducting oxide, Hyperfine Interact. **41**, 641 (1988).
[295] W. Meisel, Mössbauer spectroscopy of corrosion products, Hyperfine Interact. **45**, 73 (1989).
[296] J. Davalos *et al.*, Mössbauer study of the thermal decomposition of goethite, Hyperfine Interact. **57**, 1809 (1990).
[297] J. S. Brooks and S. Thorpe, The characterisation of iron-containing intermetallic phases within the surface region of an aluminium alloy, Hyperfine Interact. **47–48**, 159 (1989).
[298] F. J. Berry, A conversion electron Mössbauer investigation of the phosphating of iron surfaces, J. Chem. Soc. Dalton Trans. **11**, 1736 (2011).
[299] K. Nomura, Y. Ujihira, and R. Kojima, Mössbauer study of corrosion products formed on iron surfaces in aqueous solutions, in *Proceedings of Indian National Science Academy* (Indian National Science Academy, New Delhi, 1982), pp. 311–316.
[300] K. Nomura and Y. Ujihira, Studies on the formation and thermal properties of manganese phosphate coatings and hureaulite by means of conversion electron and transmission Mössbauer spectrometry, J. Mater. Sci. **17**, 3437 (1982).
[301] M. Carbucicchio, G. Palombarini, and G. Sambogna, Mössbauer study of the corrosion products on iron surfaces, Hyperfine Interact. **57**, 1775 (1990).
[302] K. Nomura and Y. Ujihira, Mössbauer spectroscopic study of iron oxides formed by pyrolysis of iron(iii) complexes, J. Anal. Appl. Pyrolysis **5**, 221 (1983).
[303] E. Matijević and J. Danon, Formation of uniform spherical iron oxides by hydrolysis of Fe(III) salts, J. Inorg. Nucl. Chem. **39**, 569 (1977).
[304] M. J. Tricker, L. A. Ash, and W. Jones, On the anomalous inertness to oxidation of the surface regions of vivianite: A $^{57}$Fe conversion electron and transmission Mössbauer study, J. Inorg. Nucl. Chem. **41**, 891 (1979).
[305] D. Hanzel, W. Meisel, and P. Götlich, Mössbauer study of iron compounds under high pressure, Hyperfine Interact. **57**, 2201 (1990).
[306] D. Hanzel, W. Meisel, D. Hanzel, and P. Gütlich, Mössbauer effect study of the oxidation of vivianite, Solid State Commun. **76**, 307 (1990).
[307] K. Nomura and Y. Ujihira, Analysis of oxalate coating on steels by conversion electron Mössbauer spectrometry, J. Mater. Sci. **18**, 1751 (1983).
[308] M. Inaba, K. Nomura, and Y. Ujihira, Changes of lattice parameter and internal magnetic field by impurity surface enrichment phenomena on Fe-36 Ni, J. Jpn. Inst. Met. **52**, 1121 (1988).
[309] M. Inaba, K. Nomura, and Y. Ujihira, Mössbauer spectra of chromium added Fe-36 Ni, J. Jpn. Inst. Met. **53**, 356 (1989).
[310] G. Fratucello, E. Colombo, O. Donzelli, and F. Ronconi, Study of the Fe-Ni interface by conversion electron Mössbauer spectroscopy, Hyperfine Interact. **45**, 255 (1989).
[311] M. Ghafari *et al.*, Magnetic studies of the new soft magnetic Fe-Ni-Cr alloys, Nucl. Instrum. Methods Phys. Res. Sect. B **76**, 37 (1993).
[312] K. Morimoto, A. Kirihigashi, and S. Nasu, Backscattering Mössbauer measurements of microstructural change in annealed duplex stainless steel, Nucl. Instrum. Methods Phys. Res. Sect. B **76**, 295 (1993).
[313] B. Boubeker, J. Eymery, M. Denanot, and E. Sayouty, A TEM and CEMS study of bcc Fe-Ni-Cr thin films, J. Magn. Magn. Mater. **133**, 470 (1994).
[314] J. Korecki and U. Gradmann, *In situ* Mössbauer analysis of hyperfine interactions near Fe(110) surfaces and interfaces, Phys. Rev. Lett. **55**, 2491 (1985).
[315] F. Volkening, B. Jonker, J. Krebs, N. Koon, and G. Prinz, Hyperfine fields and spin orientations in ($Fe^{57}$/Ag) superlattices from conversion electron Mössbauer studies, J. Appl. Phys. **63**, 3869 (1988).
[316] F. Volkening *et al.*, Magnetic relaxation effects in $^{57}$Fe, J. Phys. Colloq. **49**, C8 (1988).
[317] J. Korecki and U. Gradmann, *In-situ* conversion electron Mössbauer spectroscopy on Fe(110)-surfaces and thin films, Hyperfine Interact. **28**, 931 (1986).
[318] J. Korecki, M. Przybylski, and U. Gradmann, Thermal variation and spatial distribution of local magnetization in ultrathin Fe(110) films, J. Magn. Magn. Mater. **89**, 325 (1990).
[319] J. Korecki and U. Gradmann, Spatial oscillation of magnetic hyperfine field near the free Fe(110)-surface, Europhys. Lett. **2**, 651 (1986).
[320] G. Liu and U. Gradmann, Magnetic order near Fe(100) interfaces from Mössbauer spectroscopy, J. Magn. Magn. Mater. **118**, 99 (1993).
[321] W. A. A. Macedo and W. Keune, Magnetism of epitaxial fcc-Fe(100) films on Cu(100) investigated *in Situ* by conversion-electron Mössbauer spectroscopy in ultrahigh vacuum, Phys. Rev. Lett. **61**, 475 (1988).
[322] O. Donzelli, G. Fratucello, F. Ronconi, J. Tejada, Z. Rachid, and X. Zhang, Magnetic properties of (111) Cu/Fe multilayers, Hyperfine Interact. **68**, 303 (1992).
[323] J. Landes *et al.*, Magnetic hyperfine fields near the Fe/Cr (100, 110) interface studied by CEMS, J. Magn. Magn. Mater. **86**, 71 (1990).
[324] J. Landes *et al.*, CEMS-study of the interface in Fe/Cr multilayer systems, Hyperfine Interact. **57**, 1941 (1990).
[325] W. Sturhahn, Nuclear resonant spectroscopy, J. Phys.: Condens. Matter **16**, S497 (2004).
[326] B. W. Adams *et al.*, X-ray quantum optics, J. Mod. Opt. **60**, 2 (2013).
[327] E. E. Alp, T. M. Mooney, T. Toellner, W. Sturhahn, E. Witthoff, R. Rohlsberger, E. Gerdau, H. Homma, and M. Kentjana, Time resolved nuclear resonant scattering from $^{119}$Sn nuclei using synchrotron radiation, Phys. Rev. Lett. **70**, 3351 (1993).

[328] R. Röhlsberger, J. Bansmann, V. Senz, K. L. Jonas, A. Bettac, K. H. Meiwes-Broer, and O. Leupold, Nanoscale magnetism probed by nuclear resonant scattering of synchrotron radiation, Phys. Rev. B **67**, 245412 (2003).

[329] K. Heeg, A. Kaldun, C. Strohm *et al.*, Coherent x-ray-optical control of nuclear excitons, Nature (London) **590**, 401 (2021).

[330] F. Schaden *et al.*, Laser-induced quenching of the Th-229 nuclear clock isomer in calcium fluoride, Phys. Rev. Res. **7**, L022036 (2025).

[331] E. V. Tkalya, Features of coherent excitation of $^{229m}$Th, Nucl. Phys. A **1022**, 122428 (2022).

[332] F. F. Karpeshin, Laser assisted two-photon electron-nucleus resonance as applied to producing the $^{229m}$Th isomer, Phys. Rev. C **110**, 054307 (2024).

[333] F. Karpeshin and M. Trzhaskovskaya, Impact of the ionization of the atomic shell on the lifetime of the $^{229m}$Th isomer, Nucl. Phys. A **969**, 173 (2018).

[334] F. Karpeshin, Electron shell as a resonator, Hyperfine Interact. **143**, 79 (2002).

[335] A. Coc, P. Descouvemont, K. A. Olive, J. P. Uzan, and E. Vangioni, Variation of fundamental constants and the role of $A$=5 and $A$=8 nuclei on primordial nucleosynthesis, Phys. Rev. D **86**, 043529 (2012).

[336] M. Thoennessen, Reaching the limits of nuclear stability, Rep. Prog. Phys. **67**, 1187 (2004).

[337] M. Thoennessen, *The Discovery of Isotopes* (Springer, Switzerland, 2016).

[338] R. Röhlsberger *et al.*, Phonon damping in thin films of Fe, J. Appl. Phys. **86**, 584 (1999).

[339] S. Hu, B. Zhang, J. Xue, and H. Pang, Lattice dynamics and enhanced electron–phonon coupling of itinerant magnet $Fe_{1-x}Co_xSi$ ($x \geqslant 0.3$): A $^{57}$Fe Mössbauer spectroscopy study, J. Magn. Magn. Mater. **593**, 171842 (2024).

[340] S. Lohaus, M. Heine, P. Guzman *et al.*, A thermodynamic explanation of the Invar effect, Nat. Phys. **19**, 1642 (2023).